JGR Atmospheres

RESEARCH ARTICLE
10.1029/2020JD033544

Intra-Annual Climate Anomalies in Northwestern North America Following the 1783–1784 CE Laki Eruption

Julie Edwards[1,2], Kevin J. Anchukaitis[1,2,4], Brian Zambri[3], Laia Andreu-Hayles[4], Rose Oelkers[4], Rosanne D'Arrigo[4], and Georg von Arx[5]

[1]School of Geography, Development, and Environment, University of Arizona, Tucson, AZ, USA, [2]Laboratory of Tree-Ring Research, University of Arizona, Tucson, AZ, USA, [3]Department of Earth, Atmospheric, and Planetary Sciences, Massachusetts Institute of Technology, Cambridge, MA, USA, [4]Tree-Ring Laboratory, Lamont-Doherty Earth Observatory of Columbia University, Palisades, NY, USA, [5]Swiss Federal Institute for Forest Snow and Landscape Research WSL, Birmensdorf, Switzerland

Abstract The 1783–1784 CE Laki eruption in Iceland was one of the largest, in terms of the mass of SO_2 emitted, high-latitude eruptions in the last millennium, but the seasonal and regional climate response was heterogeneous in space and time. Although the eruption did not begin until early June, tree-ring maximum latewood density (MXD) reconstructions from Alaska suggest that the entire 1783 summer was extraordinarily cold. We use high-resolution quantitative wood anatomy, climate model simulations, and proxy systems modeling to resolve the intra-annual climate effects of the Laki eruption on temperatures over northwestern North America. We measured wood anatomical characteristics of white spruce (*Picea glauca*) trees from two northern Alaska sites. Earlywood cell characteristics of the 1783 ring are normal, while latewood cell wall thickness is significantly and anomalously reduced compared to non-eruption years. Combined with complementary evidence from climate model experiments and proxy systems modeling, these features indicate an abrupt and premature cessation of cell wall thickening due to a rapid temperature decrease toward the end of the growing season. Reconstructions using conventional annual resolution MXD likely over-estimate total growing season cooling in this year, while ring width fails to capture this abrupt late-summer volcanic signal. Our study has implications not only for the interpretation of the climatic impacts of the Laki eruption in North America, but more broadly demonstrates the importance of timing and internal variability when comparing proxy temperature reconstructions and climate model simulations. It further demonstrates the value of developing cellular-scale tree-ring proxy measurements for paleoclimatology.

Key Points:

- Quantitative wood anatomy, climate model data, and proxy systems modeling show abrupt late summer cooling in Alaska after the Laki eruption
- We show the importance of timing and internal variability when comparing proxy temperature reconstructions and climate model simulations
- Quantitative wood anatomy provides a better understanding of how traditionally used tree-ring metrics are affected by volcanic forcing

Correspondence to:
J. Edwards,
julieedwards@email.arizona.edu

Citation:
Edwards, J., Anchukaitis, K. J., Zambri, B., Andreu-Hayles, L., Oelkers, R., D'Arrigo, R., & von Arx, G. (2021). Intra-annual climate anomalies in northwestern North America following the 1783–1784 CE Laki eruption. *Journal of Geophysical Research: Atmospheres*, *126*, e2020JD033544. https://doi.org/10.1029/2020JD033544

Received 17 JUL 2020
Accepted 7 DEC 2020

1. Introduction

Volcanic eruptions are the most important natural radiative forcing on the climate system during the last millennium (Crowley, 2000; Masson-Delmotte et al., 2013; G. A. Schmidt et al., 2012). Large explosive volcanic eruptions emit sulfur into the upper troposphere and lower stratosphere, creating aerosols that reduce incoming solar radiation, altering the planet's energy balance, and cooling global mean surface temperatures (Robock, 2000; D. P. Schneider et al., 2009). They are also our only, albeit imperfect, natural analog for solar radiation management using stratospheric aerosols (Robock et al., 2013). The majority of studies on the climatic effects of volcanic eruptions have focused on the global impact of tropical eruptions, while the effects of high-latitude eruptions are less well understood but no less important (Kravitz & Robock, 2011; Pausata et al., 2015; Toohey et al., 2019). High-latitude eruptions have had a profound effect on both climate and society. An extra-tropical Northern Hemisphere eruption in 536 CE (Sigl et al., 2015) is linked to frigid temperatures, crop failures, and famine across Europe and Asia (Helama et al., 2018; Newfield, 2018) and marked the onset of the Late Antique Little Ice Age (Büntgen et al., 2016). The eruption of Alaska's Okmok volcano in 43 BCE was one of the largest high latitude volcanic eruptions of the past 2,500 years, caused widespread cooling across the Northern Hemisphere, and may have contributed to the eventual demise of the Roman Republic (McConnell et al., 2020). The 1783–1784 CE Laki eruption caused widespread mortality in Iceland and across Europe and drought in tropical Africa and Asia (Oman et al., 2006; Thordarson & Self, 2003; Zambri et al., 2019a). A better understanding of the climate impacts following volcanic eruptions allows us to prepare for the consequences of future eruptions and to evaluate the ability of climate models to

simulate the Earth system response to changes in radiative forcing (Bethke et al., 2017; Newhall et al., 2018; Robock et al., 2013; Timmreck, 2012; Zambri et al., 2019a).

Eruptions from northern high-latitude volcanoes large enough to cause significant hemisphere-scale temperature anomalies are rare, which leads to substantial uncertainty concerning their impacts. Known high-latitude eruptions associated with significant radiative forcing during the Common Era occurred in 536, 822, 939, 1,182, 1,210, 1783, and 1912 CE (Sigl et al., 2015), with only the 1912 Katmai (Novarupta) eruption in Alaska occurring during a period of widespread instrumental observations. Climate reconstructions based on paleoclimate proxy data address this limitation by providing an opportunity to increase the number of eruptions that can be analyzed. However, there remain significant discrepancies between the climate responses to volcanic eruptions in climate model simulations and those estimated from proxy reconstructions in both magnitude and duration (K. J. Anchukaitis et al., 2012; D'Arrigo et al., 2013; LeGrande & Anchukaitis, 2015; S. Stevenson et al., 2017; Stoffel et al., 2015; Wilson et al., 2016). Among the main sources of uncertainty in climate reconstructions themselves are the spatial coverage of the proxy network, the seasonal window recorded by the proxies, and biological memory and other nonclimatic or noise components of the proxy signal (K. J. Anchukaitis et al., 2012; D'Arrigo et al., 2013; Zhu et al., 2020). The precise timing of the eruption (S. Stevenson et al., 2017), the magnitude (Stoffel et al., 2015; Timmreck et al., 2009), the spatial distribution of aerosol loading (D. P. Schneider et al., 2009; Toohey & Sigl, 2017; Toohey et al., 2019), and representation of important aerosol processes (Aubry et al., 2020; LeGrande et al., 2016; Mann et al., 2015; Marshall et al., 2019; Mills et al., 2016; Pinto et al., 1989; A. Schmidt et al., 2018; Timmreck et al., 2010) are all major sources of uncertainty in model simulations. Discrepancies can also arise when comparing modeled annual temperature to climate reconstructions from high-latitude tree-ring proxy data that predominantly reflect growing season temperatures (K. J. Anchukaitis et al., 2012; D'Arrigo et al., 2013; Zhu et al., 2020). Persistent growth anomalies associated with biological memory and proxy noise are more prevalent in tree-ring width (TRW) reconstructions than maximum latewood density (MXD) reconstructions, and studies comparing modeled climate response to proxy reconstructions have found that TRW can both underestimate the volcanic cooling effect and show a lagged response (D'Arrigo et al., 2013; Esper et al., 2015; Frank et al., 2007). MXD is therefore considered the best tree-ring metric for skillfully reconstructing interannual high-latitude temperature variability, making it the most appropriate proxy when quantifying volcanic climate signals (K. J. Anchukaitis et al., 2017; Björklund et al., 2019; Esper et al., 2015, 2018). Fundamentally, some of the uncertainty in proxy-model comparisons will arise due to the chaotic nature of the climate system. The actual climate response following a volcanic eruption and recorded by proxy data is subject to internal climate variability and would not be expected to reflect simply the forced climate response represented by a climate model ensemble mean.

Here we investigate the climate impacts of the 1783–1784 CE Laki eruption in Iceland, one of the largest and most significant high-latitude eruptions of the Common Era (Sigl et al., 2015; Thordarson & Self, 2003). The Laki eruption sequence began in June 8, 1783 and did not end until February 7, 1784, emitting approximately 122 megatons SO_2 into the atmosphere (Thordarson & Self, 2003). The atmospheric pollution caused health problems and deaths from resulting respiratory disorders across Iceland and Europe (Grattan et al., 2003; A. Schmidt et al., 2011; Thordarson & Self, 2003; Witham & Oppenheimer, 2004; Zambri et al., 2019b). Historical observations indicate the eruption had a measurable effect on climate and atmospheric conditions in Europe, while few records describe the effect on climate across North America (D'Arrigo et al., 2011; Thordarson & Self, 2003). Temperature reconstructions from tree-ring MXD in Alaska indicate an extraordinarily cold growing season (between April and September) in 1783 (K. J. Anchukaitis et al., 2013; K. R. Briffa et al., 1994; Jacoby et al., 1999), despite the fact that the Laki eruption in Iceland only started in June. While summer cooling is the expected climate response to volcanic eruptions, early instrumental and documentary historical records suggest the summer of 1783 was actually abnormally warm in Europe (Luterbacher et al., 2004; Thordarson & Self, 2003). However, most temperature reconstructions using TRW and MXD indicate cooling over Europe, potentially due to the direct detrimental effect of the eruption's acidic haze on tree growth (K. R. Briffa et al., 1988; Schove, 1954). Temperature field reconstructions using a wide range of proxy observations and statistical methods also show different climate responses across the Northern Hemisphere (Figure 1). The reconstructions disagree on cooling over Europe, with Anchukaitis et al. (2017) capturing the historical observed warming over the UK, while all reconstructions would suggest colder conditions over Fennoscandia, again in contrast to historical and early

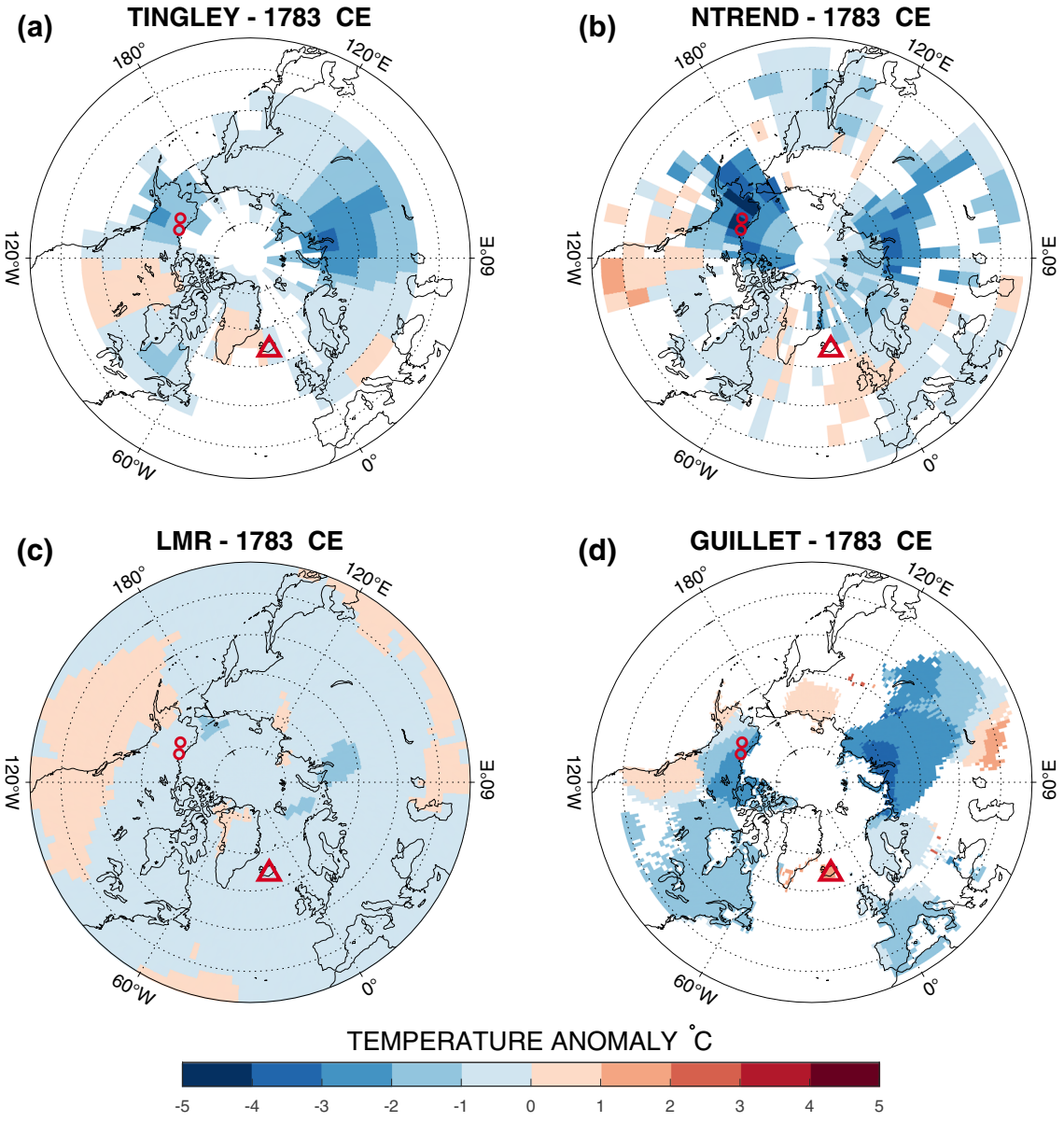

Figure 1. Proxy reconstructed temperature field anomalies in 1783 CE from (a), Tingley and Huybers (2013) (April–September), (b) Anchukaitis et al. (2017) (May–August), (c) Tardif et al. (2019) (annual), and (d) Guillet et al. (2017) (June–August). Values plotted are the temperature anomalies (°C) from the mean of reconstructed temperatures for the 3 years prior (1780–1782 CE) to the eruption at each grid point. The red triangle marks the location of the Laki volcano. Red circles mark the Firth River and Sukakpak sites.

instrumental records (Luterbacher et al., 2004; Thordarson & Self, 2003). Anchukaitis et al. (2017) and Guillet et al. (2017) show the strongest cooling over northwestern North America (Alaska and western Canada), and all reconstructions indicate warmer conditions over the western United States and northeastern Pacific (Hakim et al., 2016; Tardif et al., 2019; Tingley & Huybers, 2013). These differences arise due to distinct methodological approaches and varied proxy data networks.

To better understand and identify the precise timing of the climate response to the Laki eruption over northwestern North America, here we combine quantitative wood anatomy (QWA), climate model simulations, and proxy system modeling to examine the climate and proxy response to the eruption at a fine temporal resolution (daily-to-monthly) throughout 1783. Cell anatomical measurements across an annual ring provide evidence for the intraseasonal influence of climate on xylem development and provide higher resolution measurements than conventional X-ray densitometry (Björklund et al., 2020; Carrer et al., 2018;

Fonti et al., 2010; von Arx et al., 2016). Because tree cambial activity is highly responsive to short-term environmental changes, intra-annual climate signals are recorded in wood cellular characteristics that can better serve as records of seasonal climate conditions than TRW or MXD alone (Deslauriers et al., 2003; Fonti et al., 2010; Ziaco et al., 2014). Climate models provide an independent line of evidence for the expected ocean-atmosphere response to a volcanic eruption. Here we use modeled daily and monthly climate fields from simulations of the Laki eruption using the Community Earth System Model, version 1 (CESM1) with the Whole Atmosphere Community Climate Model (WACCM) atmospheric component, to understand the forced climate response and internal climate variability over Alaska (Zambri et al., 2019b). This model includes realistic aerosol microphysics and interactive chemistry critical for simulated volcanic eruptions (Mills et al., 2016, 2017; Pinto et al., 1989; A. Schmidt et al., 2010; Timmreck et al., 2010). Multiple ensemble members allow us to separate the forced response from internal variability (Pausata et al., 2015; Zambri et al., 2019b). Finally, proxy system models enable integration of paleoclimate proxy observations and climate model experiments by providing a forward model for simulating and interpreting the biophysical behavior of the tree-ring width proxy (M. Evans et al., 2013). Here we use a mechanistic model of tree-ring formation (K. J. Anchukaitis et al., 2020; Vaganov et al., 2006) to evaluate daily climate influence on the dynamics of tree-ring xylogenesis. This combination of independent methods and observations allows us to constrain the timing of the climate response to Laki in northwestern North America and reveals the important role of timing and internal variability when comparing paleoclimate reconstructions to climate model simulations of volcanic eruptions.

2. Methods

2.1. Quantitative Wood Anatomy

Living and subfossil wood samples of white spruce (*Picea glauca*) were collected from the Firth River at latitudinal treeline (68.65°N, 141.63°W), and from Sukakpak Mountain (67.60°N, 149.76°W) (K. J. Anchukaitis et al., 2013; D'Arrigo et al., 2014). Based on weather station data from 1977 to 2010, the Sukakpak site is in the warmer Central Interior climate division while the colder Firth River site is in the Northeast Interior division (Bieniek et al., 2012). We selected 22 cores (11 from each site) for quantitative wood anatomy (QWA) analysis that spanned the period from 1768 to 1798. The crossdated chronology, ring-width measurements, and MXD series were previously developed following standard dendrochronological procedures (K. J. Anchukaitis et al., 2013; Andreu-Hayles et al., 2011; D'Arrigo et al., 2014). We used the original raw tree-ring width measurements to verify the dating of the 1783 ring in the 22 samples used here prior to processing for QWA analysis. For this study, we also created Firth River and Sukakpak TRW chronologies by fitting a cubic smoothing spline with 50% frequency response cutoff at 30 years to the raw ring width measurements using the R-package dplR (Bunn, 2008; R Core Team, 2019).

We cut the wood samples to a thickness of 9–10 microns using a Rotary Microtome (Microm HM355S). The wood microsections were stained with a safranin/Astra Blue solution, permanently fixed in Eukitt, and prepared following standard procedures (Gärtner & Schweingruber, 2013; von Arx et al., 2016). Digital images of the microsections were produced at the Swiss Federal Research Institute WSL in Birmensdorf, Switzerland, using a Zeiss Axio Scan Z1. We measured the cell lumen area (LA) and cell wall thickness (CWT) for the period 1768–1798 CE on all samples using the ROXAS (v3.1) image analysis software (von Arx & Carrer, 2014). The cell wall thickness of all four cell walls (the two tangential and two radial walls per tracheid cell) was measured to obtain an average CWT per cell (Prendin et al., 2017). We excluded measurements of samples with cell walls damaged during sampling or preparation. A total of 754,228 tracheid cells were measured over the period 1768–1798. For analysis, we divided each ring into 10 equal increments equivalent to the percent of total width of each ring and assigned the measured cells to the corresponding increment based on their position in each ring. We then calculated the median CWT and median LA in each of these increments. Median values were used here to avoid bias due to the influence of individual outliers. We calculated anatomical MXD as the maximum ratio between the cell wall area and the total cell area (the sum of cell wall and cell lumen area) throughout the ring at a resolution of 10 μm following Björklund et al. (2020). Earlywood and latewood widths for each ring were determined by Mork's index at a 10 μm resolution (Denne, 1989; Mork, 1928). We obtained the average number of cells in a radial file across each ring

using the RAPTOR program (Peters et al., 2018). In the wood anatomical, climate simulation, and proxy simulation analyses, we distinguish between Laki (1783) and noLaki (the 15 years before and after in the QWA, or the model experiments without a simulated eruption). We used the nonparametric Mann–Whitney U test to evaluate significant differences between Laki and noLaki CWT, LA, and the relative location of the earlywood/latewood boundary. The Mann–Whitney U test evaluates the null hypothesis that two independent samples of data come from a population with equal medians. We chose this test because the Laki and noLaki QWA measurements do not have a normal distribution and the sample sizes are not equal.

2.2. Climate Model Simulations

We use the modeled daily and monthly temperature, winds, and sea level pressure (SLP) fields from the climate model experiments conducted by Zambri et al. (2019b) to investigate the range of potential climate anomalies over Alaska following the Laki eruption. Zambri et al. (2019b) use CESM1(WACCM), the high-top atmospheric component of CESM1. WACCM has 70 vertical levels, a model top of 5.1×10^{-6} hPa and 0.9° latitude x 1.25° longitude horizontal resolution, with interactive atmospheric chemistry, radiation, and dynamics, which makes it an appropriate model to use when studying the effect of volcanic aerosols on the stratosphere (Mills et al., 2017). Simulations with interactive aerosols can more realistically capture potential changes in climate variability induced by the eruption compared to simulations with prescribed aerosol loads (Mills et al., 2016). Zambri et al. (2019b) simulated the Laki eruption using the eruption characteristics described by Thordarson and Self (2003); the 1783–1784 CE Laki eruption began on June 8, 1783 and lasted for approximately 8 months. The series of eruptions injected a total of 122 Tg of SO_2 into the atmosphere, about 94 Tg into the upper troposphere/lower stratosphere, between 9 and 13 km, and another 28 Tg was emitted at the surface (Thordarson and Self, 2003). Uncertainties in the sulfur concentrations in tephra used to estimate total emissions could be upward of ±20%, however (D. S. Stevenson et al., 2003; Oman et al., 2006).

The climate model simulation experiments used here were initialized from four sets of initial conditions, each with different background states of global circulation. The four initial conditions that best matched historical observations of atmospheric conditions over Europe around June 8, 1783 were chosen from a 25-years control run. One 40-member ensemble with the Laki eruption (Laki), and another 40-member ensemble without the eruption (noLaki), were created from 10 ensemble members for each of the four initial conditions (Zambri et al., 2019b). We calculated a monthly Laki–noLaki temperature difference for each run by subtracting the noLaki mean from each individual Laki run. We adopted the procedure used by Deser et al. (2014), mapping the contributions from the forced response and the internal variability for the runs with the most negative and most positive Laki–noLaki temperature anomalies. The forced response was obtained by averaging all 40 Laki ensemble members and the internal variability was obtained by subtracting the forced response from the Laki–noLaki temperature anomaly (Deser et al., 2014). We evaluated the atmospheric circulation response using the Laki–noLaki sea level pressure (SLP) and 850-hPa wind anomalies. In addition to evaluating the full 40-member ensemble, we selected two specific members from the experiment (Run 5 and Run 40), to represent the most extreme cooling and warming, respectively, at our sites during the latter part of the growing season.

We evaluated the model's ability to reproduce absolute temperatures by comparing monthly mean temperatures at each site as simulated by the CMIP5 CESM1(WACCM) modern historical run (Marsh et al., 2013) and a CESM1(WACCM) SO_2 injection control (1975–2016) run (Mills et al., 2017) to the equivalent grid from the Climatic Research Unit (CRU) TS 4.03 temperature product (Harris et al., 2014) and the NCEP/NCAR Reanalysis (Kalnay et al., 1996). We also compared the gridded observations, Reanalysis, and the simulations with several of the closest stations in the US and Canada from the Global Historical Climatology Network (v3; Lawrimore et al., 2011). At the site-level, however, we were unable to quantify a consistent mean temperature bias between models, gridded observations, or Reanalysis, with differences in growing season temperatures varying up to several Celsius degrees colder or warmer depending on the particular paired data used for the comparison. Because of these inconsistencies, we did not apply a temperature correction to the Laki or noLaki model experiments used here. The 18th-century model bias is therefore a potential source of additional uncertainty in our climate and proxy systems modeling analyses described below.

Table 1
Results of Mann–Whitney U Test Between Laki and noLaki Measurements of Cell Wall Thickness (CWT) and Cell Lumen Area (LA)

	Firth river		Sukakpak	
% ring width	CWT *p*-value	LA *p*-value	CWT *p*-value	LA *p*-value
0–10	0.95	0.29	0.46	0.98
10–20	0.67	0.93	0.75	0.42
20–30	0.18	0.15	0.59	0.84
30–40	0.11	0.71	0.43	0.28
40–50	0.007	0.57	0.70	0.25
50–60	<0.001	0.92	0.60	0.39
60–70	<0.001	0.69	0.64	0.23
70–80	<0.001	0.29	0.08	0.49
80–90	< 0.001	0.07	<0.001	0.26
90–100	<0.001	0.02	<0.001	0.001

Note. Value shown in the columns are the significance (p-value) of the test for differences between Laki and noLaki measurements for the cells in the different relative positions of the tree rings (the % total ring width). See Methods for additional details.

2.3. Proxy Systems Modeling

We used the Vaganov–Shashkin tree-ring proxy systems model (VSM) to simulate daily cambial growth activity throughout a year under Laki conditions and a year without Laki conditions at the Sukakpak and Firth River sites (K. J. Anchukaitis et al., 2020; M. N. Evans et al., 2006; Vaganov et al., 2006). VSM relates environmental factors to daily cambial growth rates using a piecewise linear function Vaganov et al. (2011) to simulate annual ring widths and associated daily and cellular-scale outputs that can be compared with finer-scale characteristics of the annual ring (E. A. Babushkina et al., 2019; H. C. Fritts et al., 1991; Vaganov et al., 2006, 2011). The model calculates a daily relative growth rate (from 0 to 1, dimensionless) for temperature and soil moisture (itself a modeled function of precipitation, snowmelt, evapotranspiration, and soil drainage) and a minimization function causes cellular growth and division to be controlled by the most limiting environmental factor scaled by daylength. VSM models the cell formation and ring width of an idealized average tree without geometric growth trends but does not simulate cell wall thickening or wood density directly (K. J. Anchukaitis et al., 2020). While absolute cell numbers are arbitrary, reflecting the differences observed between real trees, ring-to-ring variability in these metrics reflects the changing pattern of daily growth-limiting factors (H. C. Fritts et al., 1991; Vaganov et al., 1990, 2006).

Here, daily 1783 temperature data of each site's nearest climate model grid cell from each run of the Laki and noLaki model ensembles were used as the primary temperature input. The Laki temperature curves and their counterpart noLaki temperature curves are identical to each other until the day of the eruption, June 8th (day 159). We applied a 12-days lowpass filter to the noisy daily temperature data to mimic the muted fluctuations of air temperature experienced directly by the cambium (K. J. Anchukaitis et al., 2020; M. N. Evans et al., 2006; Vaganov et al., 2006; Vermunt et al., 2012). The daily simulated precipitation output was not retained from the original climate model experiments, so we randomly selected a year of daily precipitation data from the nearest meteorological station at Dawson, Yukon Territory, Canada([Peterson & Vose, 1997) for each run of VSM. Neither our simulations nor their interpretation are sensitive to this choice, however, as growth rates in the model are dominated in all cases by temperature limitation. We used the model parameters from Evans et al. (2006), with two modifications: we set the minimum temperature for tree growth to 0°C (K. J. Anchukaitis et al., 2012, 2020; Tolwinski-Ward et al., 2013) and the temperature sum for initiation of growth to 10°C, as Alaskan white spruce are adapted to cold conditions and growth begins before complete snowmelt in May (Gregory, 1971; Vaganov et al., 2006). We ran the model to simulate tree cell growth in 1783 as a discrete year twice, using the first run only to initialize realistic starting snow and soil moisture parameters for each Laki and noLaki ensemble member. The VSM data presented here are the results from the second set of simulations. Previous applications of VSM have shown that the model can successfully reproduce patterns of interannual growth in both temperature and moisture-sensitive trees (K. Anchukaitis et al., 2006; K. J. Anchukaitis et al., 2020; Bunn et al., 2018; M. N. Evans et al., 2006; Vaganov et al., 1999, 2006, 2011).

3. Results

3.1. Quantitative Wood Anatomy

The results of the Mann–Whitney U test, used to evaluate significant differences between Laki and noLaki CWT and LA, are reported in Table 1. Latewood constitutes the last 20% of the ring for both sites during Laki and noLaki years, and the relative location of the earlywood/latewood boundary in the ring was not significantly different in Laki versus noLaki years. Latewood CWT in the Laki year (1783) is significantly lower ($p < 0.001$), than in the noLaki years at both sites. LA is only significantly higher ($p < 0.05$) in the Laki years in the last 10% of growth (Figure 3a, and 3b). CWT of the Laki year is only significantly lower than the noLaki years in the last 20% of growth for the Sukakpak site, while for the Firth River site is significantly lower

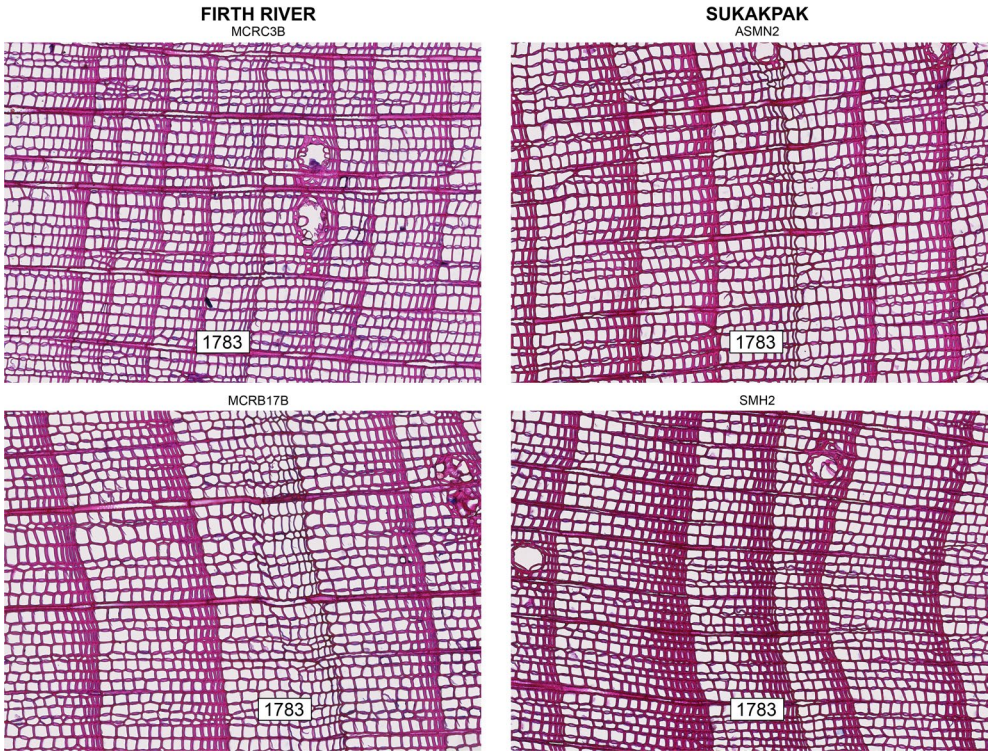

Figure 2. Example micrographs of four trees from Firth River and Sukakpak, stained with safranin/Astra blue. The eruption year 1783 is indicated in each. Three of these example trees show a typical "light ring" (D'Arrigo et al., 2014; Filion et al., 1986) or "blue ring" (Piermattei et al., 2015) structure characterized by thin cell walls throughout the latewood, while SMH2 is an example of relatively normal latewood growth until the last row of cells that have lower CWT.

in the last 60% of growth (Figure 2c, and 2d). While 1783 is generally closer to the pith in the Firth River trees and closer to the bark in Sukakpak trees, the difference in the CWT behavior between sites cannot be explained by the distinct average tree-age at each site alone. At Firth River, living trees, where 1783 is closer to the pith, and subfossil wood, where 1783 is closer to the bark, show a difference between the Laki and noLaki CWT in the last 60% of the ring. The response of the tangential CWT is less pronounced than the response of the radial CWT at both sites (Figure 3e-3h). The Firth River anatomical MXD and CWT of the last 10% of growth correlate highly ($r > 0.95$, $p < 0.001$ and $r > 0.94$, $p < 0.001$ respectively) with the existing Firth River MXD chronology from Anchukaitis et al. (2013). The average radial cell count was 13 ± 8 for noLaki years and 8 ± 2 for 1783 at Firth River, and 10 ± 4 for noLaki years and 9 ± 2 for 1783 at Sukakpak. However, for many of the Firth River samples, the 15 years prior to the eruption are close to the pith, and therefore tree geometry itself skews the average noLaki total cell count higher, with pre-eruption noLaki cell counts of 16 ± 9 and a post-eruption noLaki cell counts of 10 ± 4. We did not, however, detect any age-related trends in the LA or CWT data. The averaged cell count chronologies correlate highly ($r = 0.84$, $p < 0.001$ at Sukakpak and $r = 0.89$, $p < 0.001$ at Firth River) with the TRW chronologies at both sites. These high correlations show the intrinsic relationship between growth characteristics at cellular scale and macroscopic ring features such as TRW and MXD (Figure 4).

3.2. Climate Model Simulations

We observe a tendency across the 40-member CESM1(WACCM) experiment for a Laki-noLaki cooling across North America in September, the month in which the cell wall thickening process in the latewood is likely completed for Alaskan white spruce (Gregory, 1971; Rathgeber et al., 2016). Both August and September climate show similar responses to the eruption, therefore the choice to examine the simulation in either August or September does not affect our conclusions. The simulated late growing season climate response

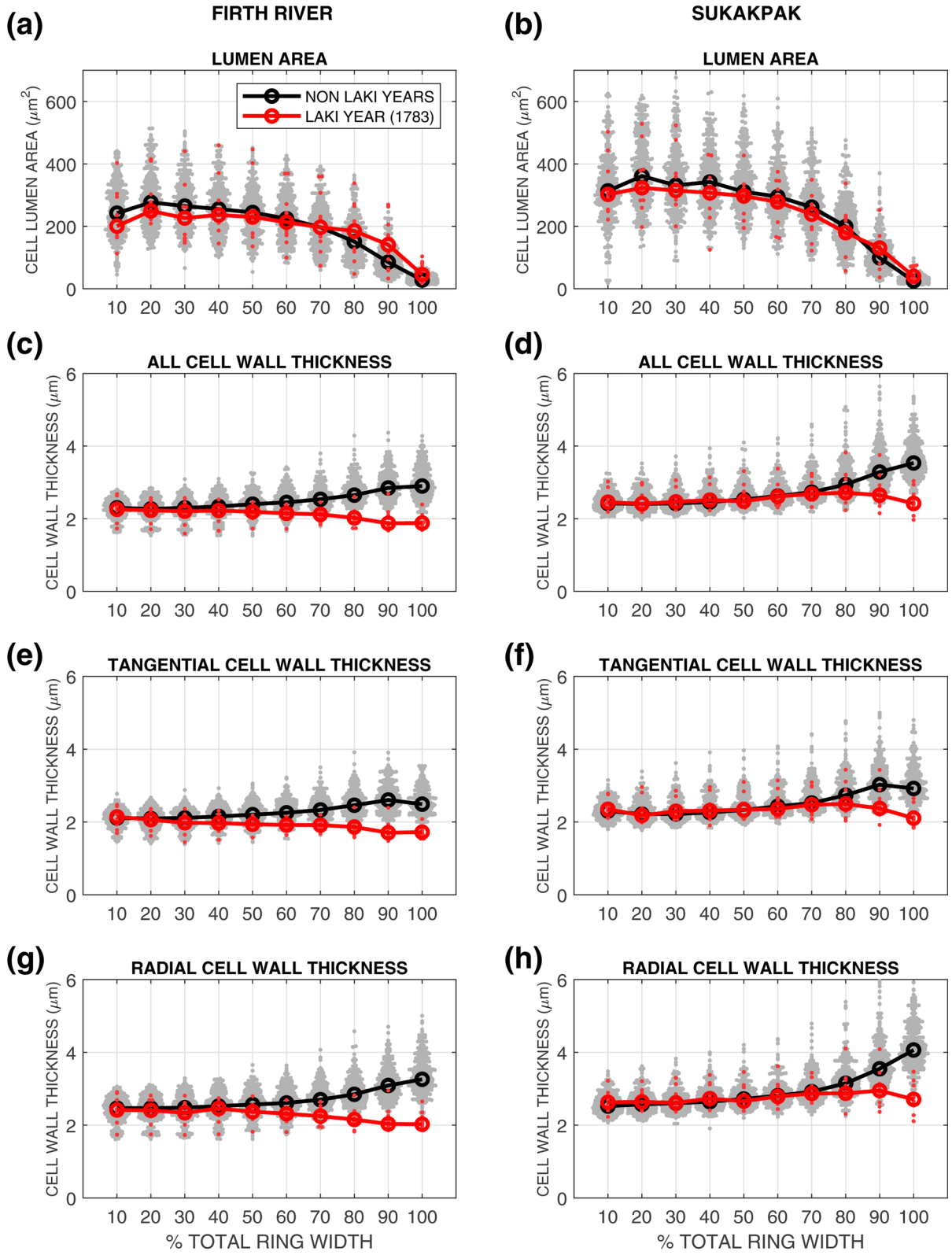

Figure 3. CWT and LA measurements for Firth River and Sukakpak. The red line indicates the overall median cell measurement for the 1783 Laki year throughout the different relative positions in the ring. The red dots represent the median cell measurement for each individual tree throughout the ring. The black line indicates the overall median cell measurement for the noLaki years. The gray dots represent the medial cell measurement for each noLaki year in each tree.

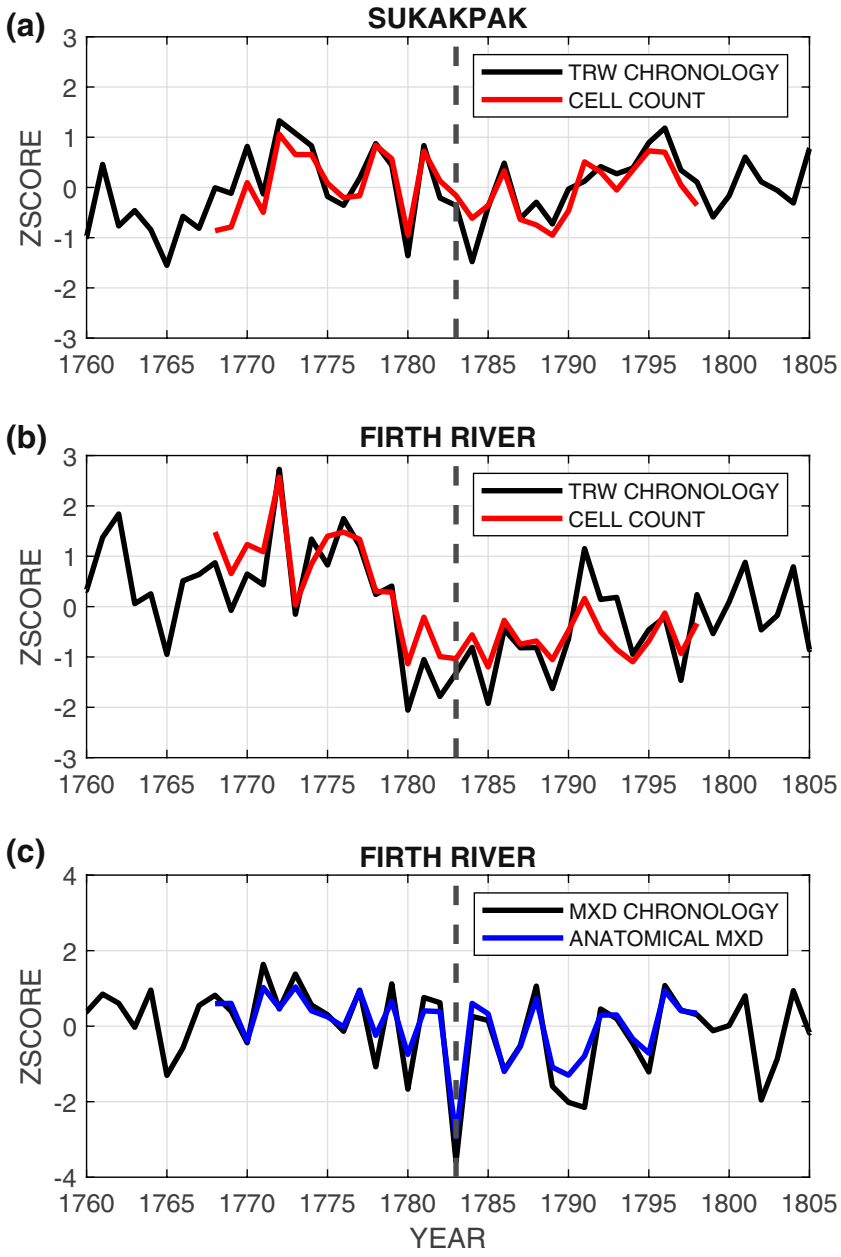

Figure 4. Tree-ring width chronologies (black line) and cell count (red line) for (a) Sukakpak and (b) Firth River (Andreu-Hayles et al., 2011). (c) Existing MXD chronology (black line) from Anchukaitis et al. (2013) and the anatomical MXD measurements (blue line, this study) for Firth River. Values are normalized for comparison of the related but different measurements (the standardized tree-ring proxy chronologies vs. the cell number or anatomical wood density from this study). The data in this study were analyzed over the period 1768–1798.

is spatially heterogeneous (Figure 5). For example, Run 5 shows ~6°C of cooling compared to the noLaki average over the Firth River and Sukakpak sites in September, while Run 40 shows up to 2°C of warming over the two sites. The average temperature anomaly of the 40 Laki–noLaki ensemble members shows that the underlying forced response is cooling, with maximum cooling of 7°C in some areas of the Arctic Archipelago and 1–2°C over the North American continent (Figure 6). Internal climate system variability in Run 5 leads to cooling over the two sites which exacerbates the forced response, while warming due to internal variability in Run 40 dominates despite the underlying forced cooling response. Indeed, Run five resembles the climate response that would be most consistent with our tree-ring data, as it simulates the average grow-

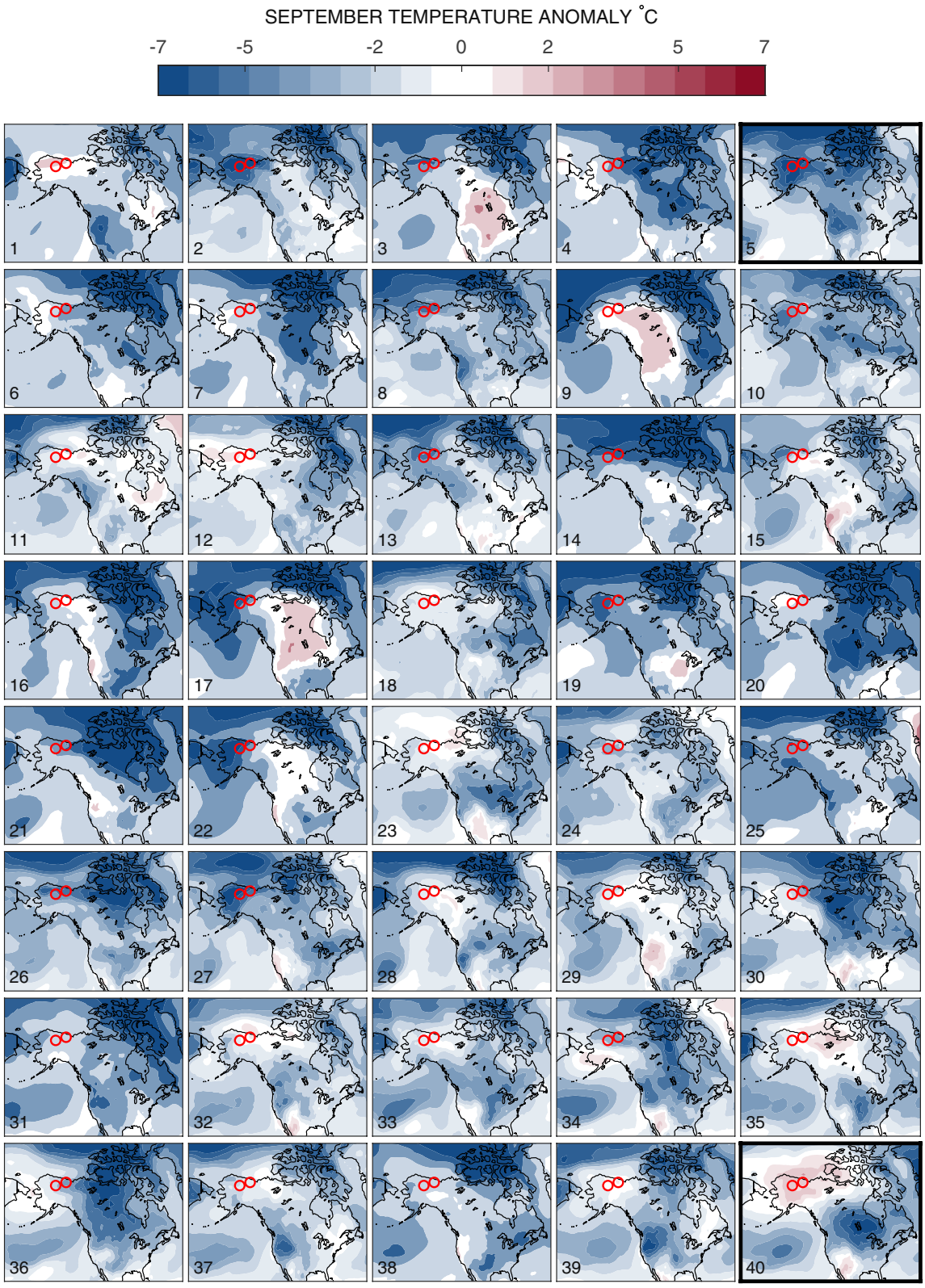

Figure 5. September Laki-noLaki temperature anomalies from each of the 40 ensemble members. Anomalies were calculated by subtracting the noLaki mean temperature field from each Laki run. Red circles mark the Firth River and Sukakpak sites.

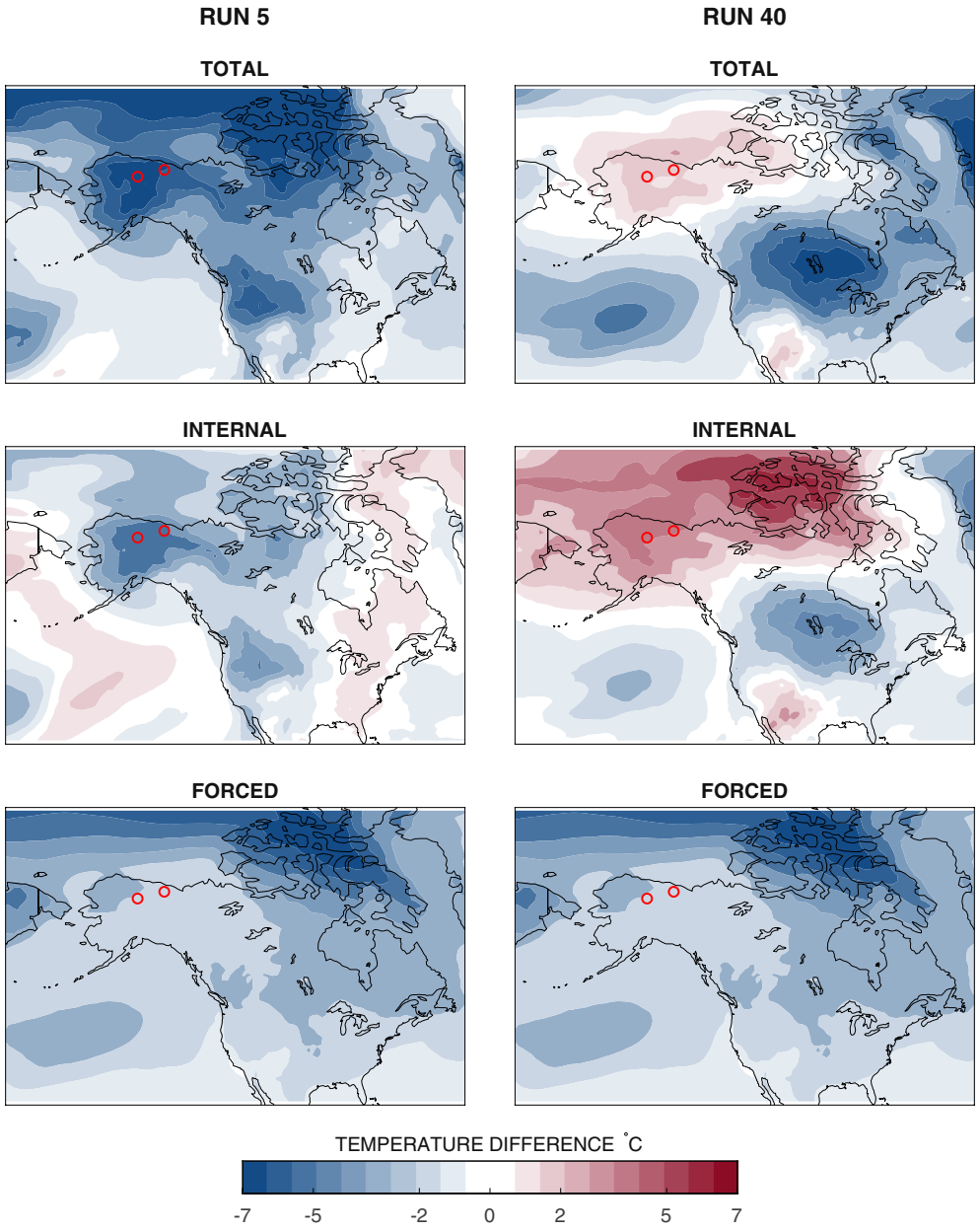

Figure 6. September Laki-noLaki temperature anomalies decomposed following Deser et al. (2014) into (middle) internal and (bottom) forced components for two opposite ensemble members, (left) Run 5 and (right) Run 40. Red circles mark the Firth River and Sukakpak sites.

ing season conditions followed by abrupt late summer cooling interpreted from the proxy data. There is a spatial gradient in the ensemble variability over Alaska; there is a wider spread of temperature anomalies in the north which then narrows in the south and along the coast (Figure 7). A positive SLP anomaly develops in September over the Bering Sea and Arctic Ocean in Run 5, with a negative SLP anomaly over Southeast Alaska; the high pressure anomaly brings cold northerly winds over Alaska.

3.3. Proxy System Modeling

The VSM results using simulated daily temperature from the CESM1(WACCM) experiment confirm that xylem formation at Firth River and Sukakpak in the late 18th century is limited primarily by temperature

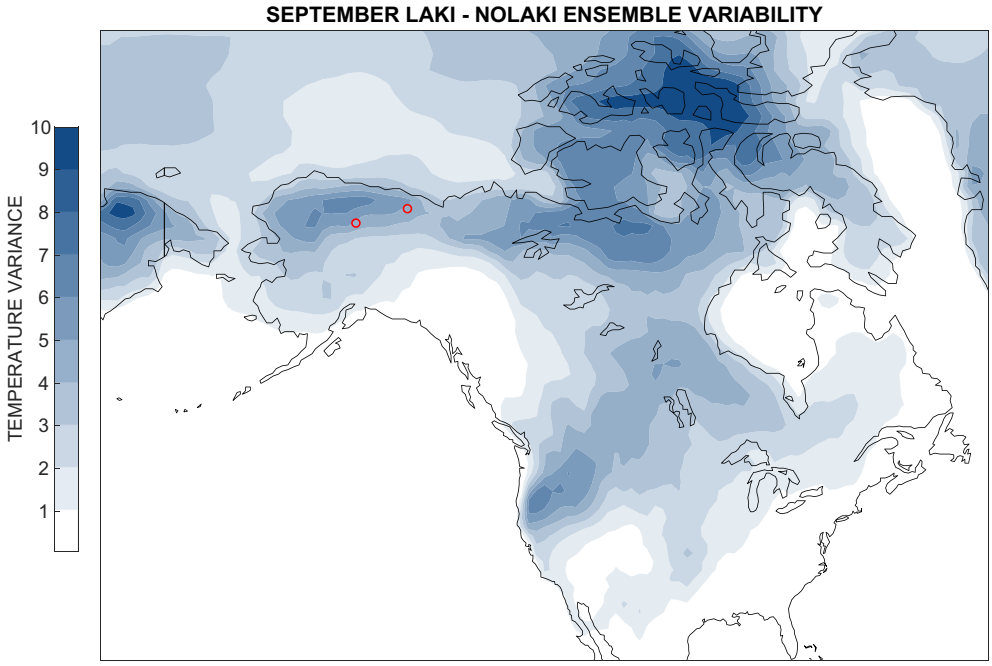

Figure 7. Variance of September Laki-noLaki temperature anomalies across the 40 ensemble members. Red circles mark the Firth River and Sukakpak sites.

with the seasonal growth pattern mediated by changes in daylength (Figure 9). For both the Laki and no-Laki scenarios, growth begins in late May at both sites. On average, simulated cell differentiation from the cambium stops at day 236 (August 24th) and day 243 (August 31st) at Sukakpak for the Laki and noLaki year respectively, with 13 ± 7 cells produced in the Laki years and 19 ± 8 in the noLaki years. At Firth River, cell differentiation from the cambium stops on average at day 237 (August 25th) and day 243 (August 31st) for the Laki and noLaki year respectively, with 10 ± 5 cells produced in the Laki years and 16 ± 6 in the noLaki years. The temperature data from Run 5 (the cold extreme scenario) produces 13 cells in the Laki annual ring at Firth River and 14 cells at Sukakpak, with the total growth rate decreasing toward the end of the growing season at both sites (Figure 10a, and 10c). The temperature data from Run 40 (the warm extreme scenario) produces a modeled cell count of 13 cells at Firth River and 26 cells at Sukakpak (Figure 10b, and 10d). The high number of simulated cells in Run 40 at Sukakpak is due to the consistently warm temperatures and therefore high growth rate throughout the entire growing season.

4. Discussion

4.1. Timing of the Laki Climate Response in Alaska

The timing and duration of the cell formation processes are important for interpreting the climate signal embedded in the cell characteristics. We can use the combination of our QWA data, proxy systems modeling, and existing knowledge of xylogenesis in high latitude conifers to constrain the timing of the cooling in Alaska associated with the Laki eruption. Based on one year of observations, Gregory (1971) concluded that May temperatures controlled the start of cell division in Alaskan white spruce, that the cambium typically reactivates before all of the winter snow is gone, and that cell division in the cambium ceased by the end of August. This is also broadly consistent with the results of our proxy systems modeling. Temperature at the beginning of the growing season is the key limiting factor for the onset of cambial activity in the xylem, and therefore influences the total number of cells that can be produced in a year (Deslauriers et al., 2008). It takes 1–2 months for a cell to fully mature after exiting the cambium (Rathgeber et al., 2016), and cell wall thickening can last up to 40–60 days for the last formed cells of the year (Rossi et al., 2008). In our VSM simulations, we observe that the cambium initiated growth in late May and cell differentiation from

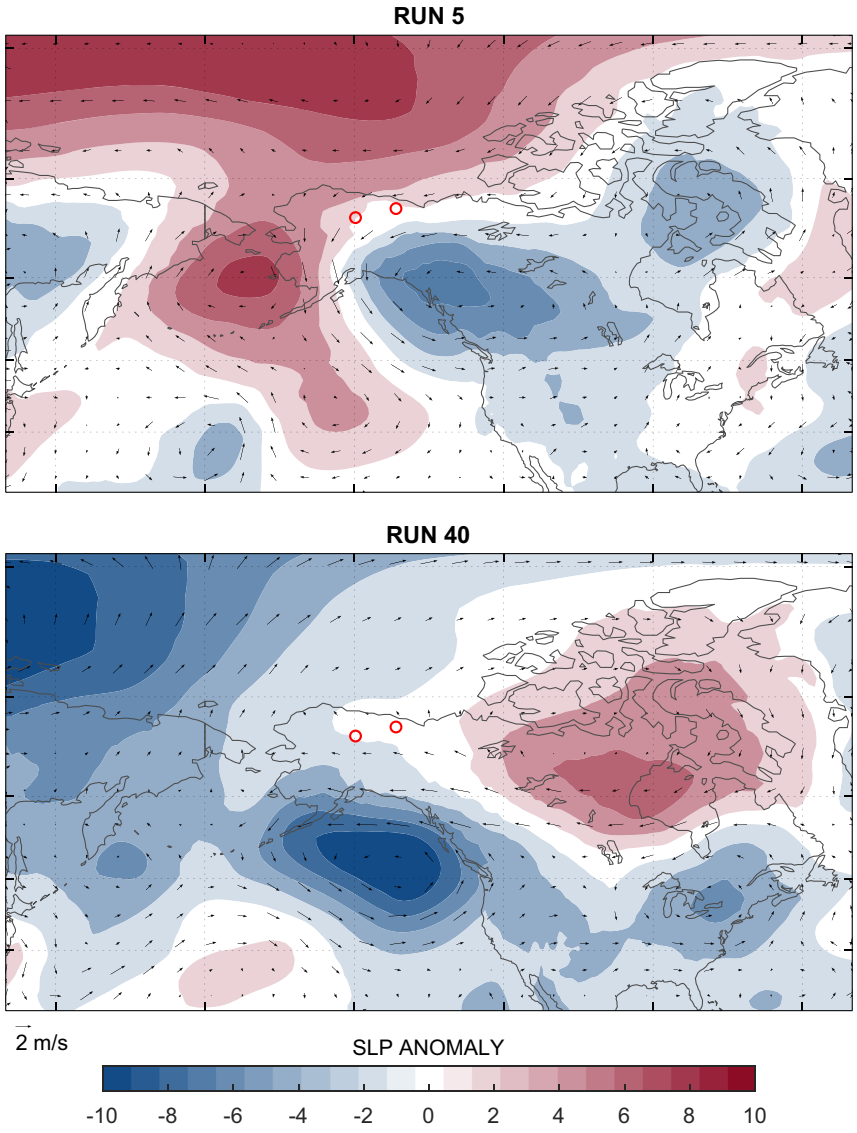

Figure 8. September Laki-noLaki SLP and wind anomalies for (left) Run 5 and (right) Run 40. SLP anomalies (hPa) are represented by filled color contours while wind anomalies are represented by vector arrows. Red circles mark the Firth River and Sukakpak sites.

the cambium ends slightly earlier but with a very large range of ensemble variability in the Laki year compared to the noLaki years, leading to a shorter growing season in VSM by 6 ± 13 days at Firth River and 7 ± 13 days at Sukakpak (Figure 9).

Importantly, however, a slightly shorter Laki growing season does not necessary affect the modeled number of cells in the simulated ring, which is consistent with our observations that ring width and cell number in 1783 are unremarkable in our tree-ring samples from the two sites. At Firth River, the modeled number of radial cells is similar between the two model runs we selected as demonstrative of the range of September climate responses (Run 5 and Run 40; Figure 10). In our QWA analysis, we found that cell count is highly correlated to TRW, which corresponds with findings in other studies (K. J. Anchukaitis et al., 2020; Lange et al., 2020; Vaganov et al., 2006). The average cell number and TRW in the Laki year show that total cell production was not negatively affected throughout most of 1783, suggesting environmental conditions during the cell production phase were normal. Early season temperatures can also influence LA, as low early summer temperature might hinder photosynthesis and therefore the cell enlargement phase (Körner, 2015).

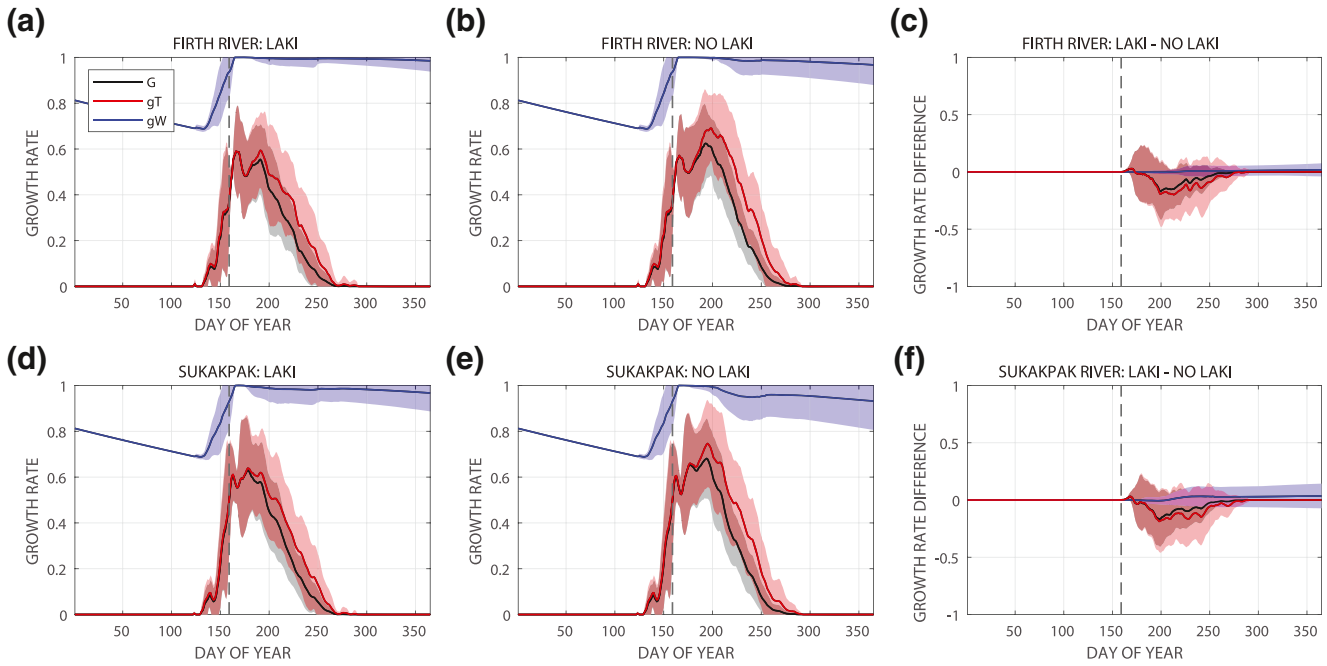

Figure 9. Simulated growth rates (0–1, dimensionless) for Firth River and Sukakpak based on the Vaganov-Shashkin tree-ring proxy systems model, averaged over the 40 (a), (d) Laki ensembles and the 40 (b),(e) noLaki ensembles. Differences between Laki and noLaki are shown in (c) and (f) for Firth and Sukakpak, respectively. The black, red, and blue lines represent the average total growth rate (g), average temperature-dependent growth rate (gT), and average moisture-dependent growth rate (gW), respectively. The shading around each mean line shows the ±1 standard deviation around the mean value. The day of the Laki eruption is indicated by the vertical dashed line.

Laki year LA is not significantly different from the noLaki LA until the last 10% of growth at both sites (Figure 3), where it is actually slightly larger in the Laki year because the thinner cell wall is less constricting on the lumen (Cuny et al., 2014). The lack of significant anomalies in TRW, LA, and earlywood CWT in 1783 collectively indicates that the early summer and probably most of the growing season of that year experienced average climate conditions.

Because cell growth appears to have proceeded as normal in the beginning and middle of the growing season, the latewood CWT measurements indicate that the climate response to the Laki eruption occurred toward the end of the summer of 1783. This truncation of the growing season primarily affected the duration of the latewood cell wall thickening process reflected by the reduced CWT (Rathgeber et al., 2016). Latewood CWT has been previously found to be positively correlated with August and September temperatures, when the cell wall thickening process is expected to occur (Carrer et al., 2016; Castagneri et al., 2017; Rossi et al., 2006, 2012), and therefore the wide separation in latewood CWT between the Laki and noLaki years at both sites (Figure 3c, and 3d) is indicative of abrupt cooling in those months. 'Light rings' (D'Arrigo et al., 2014; E. Babushkina et al., 2020; Filion et al., 1986; Gindl et al., 2000) or "blue rings" (Matisons et al., 2020; Piermattei et al., 2015) characterized by abnormally low latewood density are interpreted to be the result of an abrupt end of cell wall thickening following exceptionally low temperatures in the later part of the growing season (Figure 2).

The connection between reduced latewood CWT and anomalously cold late summer temperatures can explain the low 1783 MXD value in existing annual chronologies (K. J. Anchukaitis et al., 2013; Jacoby et al., 1999). It has been observed that the main control on latewood density is the dimensions of the cell walls (Björklund et al., 2017). The low anatomical density (calculated as the cell wall area divided by the total cell area) in 1783 arises entirely from reduced cell wall area due to small CWT, as the total cell area is not significantly different between noLaki and Laki years. Previous studies using MXD in Alaska and western Canada have found that MXD has positive correlations with monthly temperatures in the April to September range (K. J. Anchukaitis et al., 2013; Andreu-Hayles et al., 2011; K. R. Briffa et al., 1992, 2002,

2004; D'Arrigo et al., 2014), depending on the site. MXD has been interpreted to be partially determined by climate conditions during initial cell formation and enlargement, which accounts for the correlation with early growing season temperatures, while the correlation with later summer temperatures is driven by the occurrence of extremely cool or short summers (Vaganov et al., 2006; Yasue et al., 2000). A sudden period of extreme cold at the end of the growing season would be directly detrimental to the cell wall thickening process, and thus the low CWT may override any earlier imprint of the average June and July temperatures and latewood density in that year would reflect only the later August or September climate signal (Vaganov et al., 2006). The annual MXD signal in 1783 therefore reflects the significantly thinner latewood CWT that was most likely caused by rapid cooling in the late summer and an abrupt end of the growing season in August or September.

Distinct growth timing due to temperature can be seen in the differences in CWT between sites. The Laki year CWT diverges from the non-Laki years CWT earlier in the ring at Firth River than at Sukakpak (Figure 3c, and 3d). Previous studies have found that the start and end dates of conifer growth vary across elevation and latitudinal gradients; sites with higher mean temperatures generally have an earlier start and later end to growth (Cuny et al., 2018; Rossi et al., 2008, 2014, 2016). Low August temperature would affect the latewood CWT at Sukakpak, and the transition wood and latewood at Firth River. Firth River is also at treeline where trees are growing at their physiological limit and are more sensitive to temperature changes (D'Arrigo & Jacoby, 1999; Fritts, 1976). The trees at the warmer Sukakpak site may be able to tolerate a reduction in absolute temperatures when thickening of the transition wood is occurring, but this compensation likely breaks down in the latewood as colder temperatures at both sites mark the end of the summer growing season. It is also possible that the site differences in the seasonal timing of CWT anomalies could reflect the spatial heterogeneity of the climate response to the Laki eruption (e.g., Figure 5).

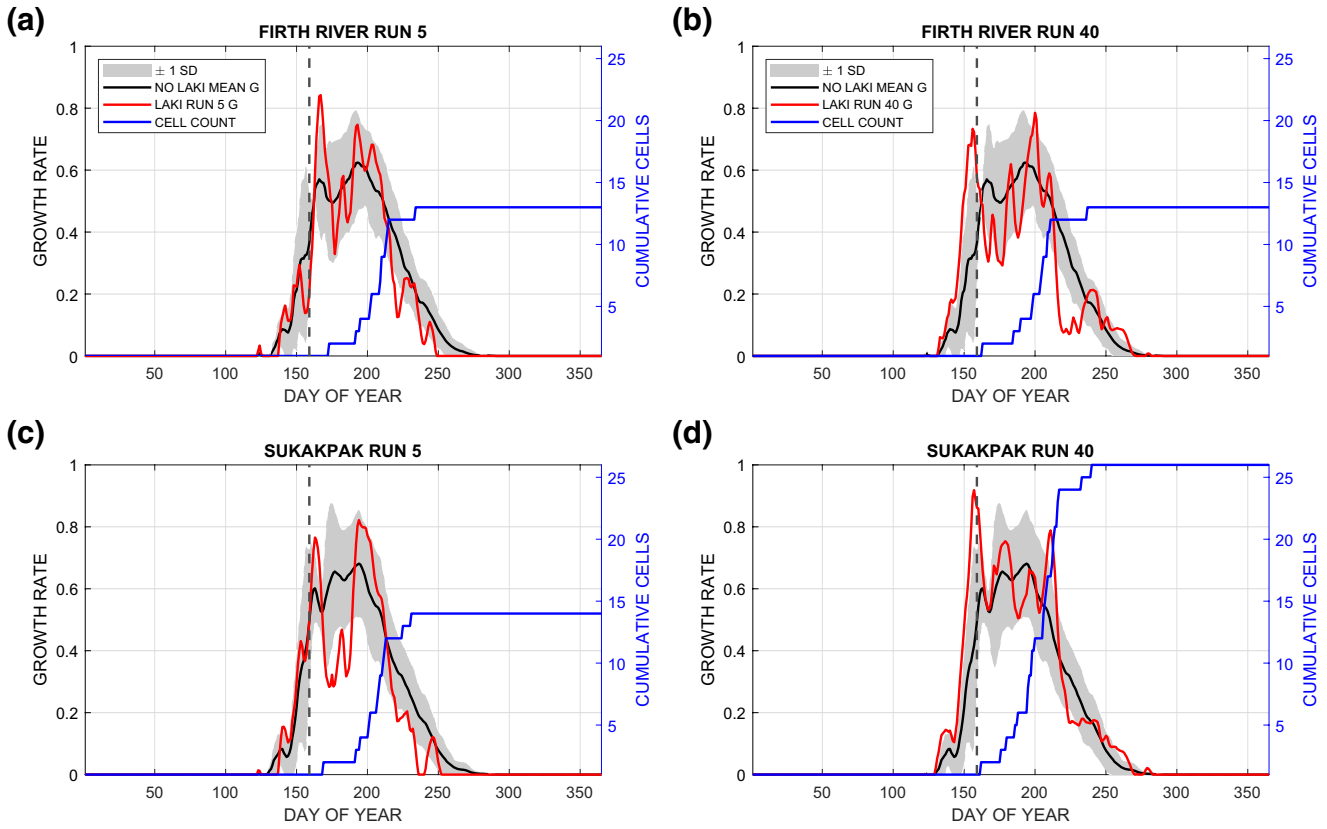

Figure 10. Simulated growth rate (0–1, dimensionless) and cumulative cell numbers at Firth River and Sukakpak for Run 5 (left) and Run 40 (right) the Vaganov-Shashkin tree-ring proxy systems model. The blue line shows the model simulated cumulative cell number (right axis) throughout the season. The red line shows the total growth rate (left axis) for each run at each site during Laki years. The black line and shading show the average noLaki total growth rate and ±1 standard deviation respectively. The day of the Laki eruption is indicated by the vertical dashed line.

4.2. Internal and Forced Variability in the Climate Response

Climate model simulations provide evidence for the timing and spatial extent of the climate response to the Laki eruption that is, independent of our proxy observations and provide complementary information for interpreting the proxy record. The availability of ensemble experiments allows the separation of the forced surface temperature response to volcanic eruption from the natural variability at a regional scale (Deser et al., 2014; Pausata et al., 2015). In our study here, the 40 ensemble members show a range of spatiotemporal climate responses following the Laki eruption (Figure 5), each reflecting a combination of the underlying forced cooling response and internal climate variability (Figure 6), and while the forced response over our study region is indeed summer cooling, the magnitude of internal variability can overwhelm this and in some members actually leads to a net warming in late summer over northern Alaska, as illustrated in Run 40 (Figure 6). The remarkably thin latewood CWT at both of our study sites in 1783 is the result of a specific spatiotemporal climate response to the Laki eruption, most likely similar to the climate response seen in Run 5. Because our proxy data come from terrestrial high latitudes where our model simulations produce a range of cooling patterns and magnitudes across the ensemble members (Figures 5 and 7), considering internal variability in proxy-climate comparisons is important.

In addition to the direct temperature effect from shortwave forcing, volcanic eruptions can perturb atmospheric circulation (DallaSanta et al., 2019; D'Arrigo et al., 2013; Driscoll et al., 2012; Liu et al., 2017; Robock, 2000; Stenchikov et al., 2006; Zanchettin et al., 2012). As shown above, different ensemble members produce different climate anomalies in response to the imposed forcing of the Laki eruption (Figure 5) and these are linked to concomitant circulation anomalies. In Run 5, the run with extreme late summer cooling, northerly wind anomalies (Figure 8) result in colder summer temperatures in interior Alaska and the Yukon Territory (Szeicz, 1996). Historical accounts also suggest a possible polar air mass incursion over Alaska following the Laki eruption, with northerly winds and 'The Time Summer Time Did Not Come' in interior Alaska at approximately the time period of the Laki eruption described in Oquilluk (1973), a collection of oral histories from the Kawerak people (Jacoby et al., 1999). Trees at latitudinal treeline are expected to be particularly sensitive to cold air incursions (D'Arrigo & Jacoby, 1999), so it is likely that our QWA data reflect the circulation anomaly that led to the intrusion of a northerly polar air mass and rapid late summer cooling.

Spatially variable regional temperature anomalies following volcanic eruptions may be broadly reflected in the different temperature reconstructions across northwestern North America (e.g., K. J. Anchukaitis et al., 2017; D'Arrigo et al., 2014; Jacoby et al., 1999). Briffa et al. (1994) observed that the most severe temperature response to the Laki eruption was in central Alaska, while southern Alaska had a milder response. D'Arrigo et al. (2004) found that temperatures decreased over the Seward Peninsula following the Laki eruption, but that the cooling was not as extreme as that inferred for interior Alaska. Thus while climate model simulations confirm that the forced response over our study region would be a surface cooling, different ensemble members show different temperature responses even at the site level within model resolution (Figure 5). As suggested above, these spatial gradients in the magnitude and even sign of the temperature response (Figure 5) could further explain some of the differences in QWA measurements between our two sites (Figure 3).

4.3. Implications for Proxy-Model Comparisons

Eruption timing and the seasonality of the resulting climate impacts are important to consider when reconciling model simulations and proxy reconstructions (Fischer et al., 2007; S. Stevenson et al., 2017). Our high-resolution cell anatomical measurements give us intra-seasonal signals of the climate response to the eruption, and the timing of the different cell formation processes provide additional information for unraveling the timing of the climate response. Cell production and enlargement processes in Firth River and Sukakpak white spruce trees in 1783 resulted in an average number of cells and average LA, indicative of normal early and mid-summer growing conditions, while the increasingly low CWT indicates later summer cooling until an abrupt end of the growing season. In this study the abrupt end of the growing season embeds a strong climate signal in the latewood CWT, which is translated to the annual MXD metric. While previous studies have used MXD temperature reconstructions to accurately reconstruct the cooling effect of

volcanic eruptions (K. R. Briffa et al., 1998; D'Arrigo & Jacoby, 1999; D'Arrigo et al., 2004; Esper et al., 2015; L. Schneider et al., 2017), our cellular-scale measurements here demonstrate that the timing of eruptions is an important consideration when interpreting MXD chronologies. The intra-annual and multivariate information available from QWA provides an opportunity to refine knowledge about the timing of post-eruption cooling and suggest improved seasonal comparisons with climate model simulations. It is also possible to incorporate this intra-annual information directly into data assimilation approaches to climate reconstruction (Tardif et al., 2019). The lack of a Laki volcanic signal in TRW chronologies and total cell numbers from our two sites may in part reflect lagged signals known to occur in TRW chronologies (c.f. D'Arrigo et al., 2013; Esper et al., 2015; Frank et al., 2007); however, our simulations provide evidence that average TRW in 1783 could be simply caused by normal early summer temperatures alone, as our VSM results suggest the xylem cells could have already formed by the time the eruption's impact would have be severe enough to affect cell division and maturation. The different stages and timing of cell formation are reflected in the different proxies often used in proxy-climate comparisons, but their interpretation can also potentially provide additional information on the specific timing of the eruption's climate impacts.

A number of studies have hypothesized that there could be an additional effect on tree growth due to changes in light availability for photosynthesis following an eruption. Robock (2005) suggested that an increase in diffuse radiation caused by light scattering by volcanic aerosols could lead to more efficient photosynthesis (Gu et al., 2003), a reduced sensitivity of tree growth to subsequent temperature anomalies, and therefore an underestimation of the total cooling due to volcanic eruptions. However, Krakauer and Randerson (2003) found no evidence of this effect across the global tree-ring network, suggesting that if such a mechanism did exist, the growth stimulation was entirely offset by the direct climatic consequences of eruptions. Photosynthesis in open-canopy forests like the Sukakpak and Firth River sites is also unlikely to benefit from increased diffuse radiation in that same way as forests with dense canopies (D'Arrigo et al., 2013; Roderick et al., 2001). In contrast to Robock (2005); Tingley et al. (2014) suggested that tree-ring proxies overestimated the amount of cooling following volcanic eruptions due to the reduction in light and a decline in biological productivity. However, the Firth River and Sukakpak sites are considered temperature—and not radiation—limited regions (Nemani, 2003; Tingley et al., 2014) and Alaskan temperature reconstructions do not show a consistent bias compared to observations following known eruptions (K. J. Anchukaitis et al., 2017; Tingley et al., 2014). Körner (1998, 2003) furthermore concluded that trees at Alpine treeline were not limited by carbon availability or photosynthetic rate, but rather directly by temperature through sink-meditated processed in the cambium. Our results here collectively demonstrate that apparently excessive cooling in some reconstructions (c.f. Tingley et al., 2014) could arise simply from the timing of an abrupt cooling event and its effect on the annual ring's MXD value. For the 1783–1784 CE Laki eruption, the annual MXD value may appear to overestimate the effect from cooling in 1783 at some sites simply because low MXD is capturing an abrupt extreme event in the late summer but is used within climate reconstructions to estimate the temperature over the entire summer. Further research using modern ecological and biogeochemical observations is needed to determine if indeed there are any collinear or confounding temperature and light effects on tree-ring proxies in response to volcanic eruptions (D'Arrigo et al., 2013).

Model simulations of tropical and high-latitude eruptions during the last millennium actually show a more pronounced volcanic cooling signal than proxy reconstructions using MXD (Masson-Delmotte et al., 2013; L. Schneider et al., 2017; Stoffel et al., 2015; Wilson et al., 2016). Overestimation of volcanic cooling in climate models can be due to unknown eruption season or location, simplified or inaccurate simulation of aerosol microphysics, and uncertainty in SO_2 injection amount and heights (LeGrande et al., 2016; Timmreck et al., 2009; Stoffel et al., 2015). While there are still uncertainties concerning the SO_2 injection heights, the location and timing of the Laki eruption are reasonably well known and are applied in the model experiments used here. As we demonstrate, there is a large amount of variability in the possible climate states following the Laki eruption (Figure 5). Any one of these states could reflect the climate anomalies that lead to a hypothetical proxy observation. The proxy data are subject to internal climate variability but are usually compared against the forced climate response in the form of an ensemble mean or a multimodel average, which conflates internal variability and structural differences between models (Deser et al., 2014). Internal climate variability needs to be considered in proxy-climate comparisons to better understand whether or not a specific model may be structurally overestimating volcanic cooling.

5. Conclusion

Volcanic eruptions are one of the most important natural climate forcings, particularly over the late Holocene. Despite this, models and proxy reconstructions disagree about the extent and timing of cooling. To resolve discrepancies between modeled volcanic forcing and proxy observations, we find that QWA measurements can provide novel information beyond that available from annual MXD or TRW values alone. Specifically, high-resolution QWA data can identify the precise timing of cooling within the growing season, potentially be used to quantify temperature anomalies during narrower periods of the growing season, and differentiate between overall growing season cooling and transient cold events following eruptions. The seasonal information revealed by QWA can also be incorporated directly in proxy systems modeling within data assimilation approaches to climate field reconstruction (Tardif et al., 2019). Previous mismatches between modeled volcanic forcing and proxy observations have been traced in part to the type of proxy data used (Esper et al., 2015; Zhu et al., 2020). MXD is still considered the most appropriate proxy to detect volcanic cooling signals and provides the most robust temperature reconstructions, but calibration of the proxy with the instrumental record necessarily assumes that it directly or indirectly reflects temperatures integrated over the entire summer or extended growing season. By investigating the cell characteristics throughout the 1783 ring, it becomes clear that growth in that year was not negatively affected by cold anomalies until later in the growing season. Our multi-method approach here shows that the severely low MXD in 1783 in at least some Alaskan tree-ring chronologies is a result of a rapid late-summer cooling and is unlikely to be representative of the rest of the growing season that preceded it. In the case of the Laki eruption, which began in June, MXD reconstructions probably overestimate the duration and magnitude of the cooling over northern Alaska when calibrated against average summer temperatures. Beyond improving spatial coverage of MXD networks (K. J. Anchukaitis et al., 2017; Esper et al., 2018; Zhu et al., 2020), a better understanding of the growth-environment relationship is needed to understand how trees as proxies record volcanic forcing. QWA provides a valuable new tool for more precisely quantifying the timing and magnitude of the climate response to volcanism, and long continuous QWA chronologies could help support more accurate reconstructions of last millennium.

Data Availability Statement

The tree-ring data that support the findings of this study are available within the article's supplementary materials and will be available in the International Tree-Ring Data Bank (ITRDB) at the NOAA/World Data Service for Paleoclimatology archives upon publication. We would like to acknowledge high-performance computing support from Yellowstone provided by the National Center for Atmospheric Research's Computational and Information Systems Laboratory, sponsored by the NSF. The model output used here is available at https://doi.org/10.7910/DVN/G1H3AC. Additional model output for CESM1(WACCM) historical simulations are available from the Earth System Grid (https://www.earthsystemgrid.org/). CRU TS high resolution gridded climate data are available from the Climatic Research Unit (https://crudata.uea.ac.uk/cru/data/hrg/). NCEP/NCAR Reanalysis fields are available from the NOAA Physical Sciences Laboratory (https://psl.noaa.gov/data/gridded/data.ncep.reanalysis.html).

Acknowledgments
We thank Kiyomi Morino and Malcolm Hughes at the Laboratory of Tree-Ring Research for establishing and supporting laboratory facilities for wood anatomy analyses and measurements at the University of Arizona, as well as for advice and guidance on sample preparation and analysis. Alberto Reyes, Angela Allen, and Susy Ellison provided excellent field assistance. KJA was supported by the Climate Program Office of the National Oceanographic and Atmospheric Administration (NA18OAR4310420) and NSF grants PLR-0902051, AGS-1159430, and AGS-1501834. BZ was supported by NSF grants AGS-1539972 and AGS-1848863. RDD, LAH, and RO additionally acknowledge NSF grants PLR-1504134, PLR-1603473 and AGS-1502150. GvA was supported by the Swiss National Science Foundation SNSF (grant no. 200021_182398, XELLCLIM). This is LDEO Contribution 8468.

References

Anchukaitis, K. J., Breitenmoser, P., Briffa, K. R., Buchwal, A., Büntgen, U., Cook, E. R., et al. (2012). Tree rings and volcanic cooling. *Nature Geoscience*, *5*(12), 836–837.

Anchukaitis, K. J., D'Arrigo, R., Andreu-Hayles, L., Frank, D. C., Verstege, A., Curtis, A., et al. (2013). Tree-ring-reconstructed summer temperatures from northwestern North America during the last nine centuries. *Journal of Climate*, *26*(10), 3001–3012. https://doi.org/10.1175/jcli-d-11-00139.1

Anchukaitis, K. J., Evans, M. N., Hughes, M. K., & Vaganov, E. A. (2020). An interpreted language implementation of the Vaganov-Shashkin tree-ring proxy system model. *Dendrochronologia*, *60*(125677). https://doi.org/10.1016/j.dendro.2020.125677

Anchukaitis, K. J., Evans, M. N., Kaplan, A., Vaganov, E. A., Hughes, M. K., Grissino-Mayer, H., et al. (2006). Forward modeling of regional scale tree-ring patterns in the southeastern United States and the recent influence of summer drought. *Geophysical Research Letters*, *33*(4). https://doi.org/10.1029/2005GL025050

Anchukaitis, K. J., Wilson, R., Briffa, K. R., Büntgen, U., Cook, E. R., D'Arrigo, R., et al. (2017). Last millennium Northern Hemisphere summer temperatures from tree rings: Part II, spatially resolved reconstructions. *Quaternary Science Reviews*, *163*, 1–22.

Andreu-Hayles, L., D'Arrigo, R., Anchukaitis, K. J., Beck, P. S., Frank, D. C., & Goetz, S. (2011). Varying boreal forest response to arctic environmental change at the Firth River, Alaska. *Environmental Research Letters*, *6*(4), 503.

Aubry, T. J., Toohey, M., Marshall, L., Schmidt, A., & Jellinek, A. M. (2020). A new volcanic stratospheric sulfate aerosol forcing emulator (EVA_H): Comparison with interactive stratospheric aerosol models. *Journal of Geophysical Research: Atmospheres*, *125*(3), e2019JD031,303. https://doi.org/10.1029/2019JD031303

Babushkina, E. A., Belokopytova, L. V., Zhirnova, D. F., & Vaganov, E. A. (2019). Siberian spruce tree ring anatomy: imprint of development processes and their high-temporal environmental regulation. *Dendrochronologia*, *53*, 114–124.

Babushkina, E. A., Zhirnova, D., Belokopytova, L., & Vaganov, E. A. (2020). Warming induced changes in wood matter accumulation in tracheid walls of spruce. *Journal of Mountain Science*, *17*(1), 16–30.

Bethke, I., Outten, S., Otterå, O. H., Hawkins, E., Wagner, S., Sigl, M., et al. (2017). Potential volcanic impacts on future climate variability. *Nature Climate Change*, *7*(11), 799–805.

Bieniek, P. A., Bhatt, U. S., Thoman, R. L., Angeloff, H., Partain, J., Papineau, J., et al. (2012). Climate divisions for Alaska based on objective methods. *Journal of Applied Meteorology and Climatology*, *51*(7), 1276–1289. https://doi.org/10.1175/JAMC-D-11-0168.1

Björklund, J., Arx, G., Nievergelt, D., Wilson, R., den Bulcke, J. V., Günther, B., et al. (2019). Scientific merits and analytical challenges of tree-ring densitometry. *Reviews of Geophysics*, *57*(4), 1224–1264. https://doi.org/10.1029/2019rg000642

Björklund, J., Seftigen, K., Fonti, P., Nievergelt, D., & von Arx, G. (2020). Dendroclimatic potential of dendroanatomy in temperature-sensitive pinus sylvestris. *Dendrochronologia*, *60*, 125673. https://doi.org/10.1016/j.dendro.2020.125673

Björklund, J., Seftigen, K., Schweingruber, F., Fonti, P., von Arx, G., Bryukhanova, M. V., et al. (2017). Cell size and wall dimensions drive distinct variability of earlywood and latewood density in northern hemisphere conifers. *New Phytologist*, *216*(3), 728–740. https://doi.org/10.1111/nph.14639

Briffa, K. R., Jones, P. D., Pilcher, J. R., & Hughes, M. K. (1988). Reconstructing summer temperatures in northern Fennoscandinavia back to A.D. 1700 using tree-ring data from scots pine. *Arctic and Alpine Research*, *20*(4), 385–394.

Briffa, K. R., Jones, P. D., & Schweingruber, F. H. (1992). Tree-ring density reconstructions of summer temperature patterns across western North America since 1600. *Journal of Climate*, *5*, 735–754.

Briffa, K. R., Jones, P. D., & Schweingruber, F. H. (1994). Summer temperatures across northern North America: Regional reconstructions from 1760 using tree-ring densities. *Journal of Geophysical Research*, *99*(D12), 25835–25844. https://doi.org/10.1029/94jd02007

Briffa, K. R., Jones, P. D., Schweingruber, F. H., & Osborn, T. J. (1998). Influence of volcanic eruptions on Northern Hemisphere summer temperature over the past 600 years. *Nature*, *393*(6684), 450–455. https://doi.org/10.1038/30943

Briffa, K. R., Osborn, T., & Schweingruber, F. (2004). Large-scale temperature inferences from tree rings: A review. *Global and Planetary Change*, *40*(1–2), 11–26. https://doi.org/10.1016/s0921-8181(03)00095-x

Briffa, K. R., Osborn, T. J., Schweingruber, F. H., Jones, P. D., Shiyatov, S. G., & Vaganov, E. A. (2002). Tree-ring width and density data around the Northern Hemisphere: Part 1, local and regional climate signals. *The Holocene*, *12*(6), 737–757. https://doi.org/10.1191/0959683602hl587rp

Bunn, A. G. (2008). A dendrochronology program library in R (dplR). *Dendrochronologia*, *26*(2), 115–124. https://doi.org/10.1016/j.dendro.2008.01.002

Bunn, A. G., Salzer, M. W., Anchukaitis, K. J., Bruening, J. M., & Hughes, M. K. (2018). Spatiotemporal variability in the climate growth response of high elevation bristlecone pine in the White Mountains of California. *Geophysical Research Letters*, *45*(24), 13–312.

Büntgen, U., Myglan, V. S., Ljungqvist, F. C., McCormick, M., Di Cosmo, N., Sigl, M., et al. (2016). Cooling and societal change during the Late Antique Little Ice Age from 536 to around 660 AD. *Nature Geoscience*, *9*(3), 231–236.

Carrer, M., Brunetti, M., & Castagneri, D. (2016). The imprint of extreme climate events in century-long time series of wood anatomical traits in high-elevation conifers. *Frontiers in Plant Science*, *7*. https://doi.org/10.3389/fpls.2016.00683

Carrer, M., Unterholzner, L., & Castagneri, D. (2018). Wood anatomical traits complex temperature influence on Pinus cembra at high elevation in the Eastern Alps. *International Journal of Biometeorology*, *62*(9), 1745–1753. https://doi.org/10.1007/s00484-018-1577-4

Castagneri, D., Fonti, P., von Arx, G., & Carrer, M. (2017). How does climate influence xylem morphogenesis over the growing season? insights from long-term intra-ring anatomy in Picea abies. *Annals of Botany*, *119*(6), 1011–1020. https://doi.org/10.1093/aob/mcw274

Crowley, T. J. (2000). Causes of climate change over the past 1000 years. *Science*, *289*, 270–277.

Cuny, H. E., Fonti, P., Rathgeber, C. B. K., Arx, G., Peters, R. L., & Frank, D. C. (2018). Couplings in cell differentiation kinetics mitigate air temperature influence on conifer wood anatomy. *Plant, Cell & Environment*, *42*(4), 1222–1232. https://doi.org/10.1111/pce.13464

Cuny, H. E., Rathgeber, C. B. K., Frank, D. C., Fonti, P., & Fournier, M. (2014). Kinetics of tracheid development explain conifer tree-ring structure. *New Phytologist*, *203*(4), 1231–1241. https://doi.org/10.1111/nph.12871

DallaSanta, K., Gerber, E. P., & Toohey, M. (2019). The circulation response to volcanic eruptions: The key roles of stratospheric warming and eddy interactions. *Journal of Climate*, *32*(4), 1101–1120.

Denne, M. (1989). Definition of latewood according to Mork (1928). *IAWA Journal*, *10*(1), 59–62.

Deser, C., A. S. Phillips, M. A. Alexander, & B. V. Smoliak (2014). Projecting North American climate over the next 50 years: Uncertainty due to internal variability. *Journal of Climate*, *27*(6), 2271–2296, https://doi.org/10.1175/jcli-d-13-00451.1

Deslauriers, A., Morin, H., & Begin, Y. (2003). Cellular phenology of annual ring formation of Abies balsamea in the Quebec boreal forest (Canada). *Canadian Journal of Forest Research*. *33*(2), 190–200.

Deslauriers, A., Rossi, S., Anfodillo, T., & Saracino, A. (2008). Cambial phenology, wood formation and temperature thresholds in two contrasting years at high altitude in southern Italy. *Tree Physiology*, *28*(6), 863–871.

Driscoll, S., Bozzo, A., Gray, L. J., Robock, A., & Stenchikov, G. (2012). Coupled Model Intercomparison Project 5 (CMIP5) simulations of climate following volcanic eruptions. *Journal of Geophysical Research: Atmospheres*, *117*(D17). https://doi.org/10.1029/2012JD017607

D'Arrigo, R., Davi, N., Jacoby, G., Wilson, R., & Wiles, G. (2014). *Dendroclimatic studies: Tree growth and climate change in northern forests*. John Wiley & Sons.

D'Arrigo, R., & Jacoby, G. (1999). Northern North American tree-ring evidence for regional temperature changes after major volcanic events. *Climatic Change*, *41*(1), 1–15. https://doi.org/10.1023/a:1005370210796

D'Arrigo, R., Mashig, E., Frank, D. C., Jacoby, G., & Wilson, R. (2004). Reconstructed warm season temperatures for Nome, Seward Peninsula, Alaska. *Geophysical Research Letters*, *31*(9). https://doi.org/10.1029/2004gl019756

D'Arrigo, R., Seager, R., Smerdon, J. E., LeGrande, A. N., & Cook, E. R. (2011). The anomalous winter of 1783–1784: Was the Laki eruption or an analog of the 2009–2010 winter to blame?. *Geophysical Research Letters*, *38*(5). https://doi.org/10.1029/2011GL046696

D'Arrigo, R., Wilson, R., & Anchukaitis, K. J. (2013). Volcanic cooling signal in tree ring temperature records for the past millennium. *Journal of Geophysical Research: Atmospheres*, *118*(16), 9000–9010. https://doi.org/10.1002/jgrd.50692

Esper, J., George, S. S., Anchukaitis, K., D'Arrigo, R., Ljungqvist, F. C., Luterbacher, J., et al. (2018). Large-scale, millennial-length temperature reconstructions from tree-rings. *Dendrochronologia*, *50*, 81–90.

Esper, J., Schneider, L., Smerdon, J. E., Schöne, B. R., & Büntgen, U. (2015). Signals and memory in tree-ring width and density data. *Dendrochronologia*, *35*, 62–70. https://doi.org/10.1016/j.dendro.2015.07.001

Evans, M. N., Reichert, U., Kaplan, A., Anchukaitis, K. J., Vaganov, E. A., Hughes, M. K., et al. (2006). A forward modeling approach to paleoclimatic interpretation of tree-ring data. *Journal of Geophysical Research*, *111*(G3). https://doi.org/10.1029/2006jg000166

Evans, M. N., Tolwinski-Ward, S., Thompson, D., & Anchukaitis, K. (2013). Applications of proxy system modeling in high resolution paleoclimatology. *Quaternary Science Reviews*, *76*, 16–28. https://doi.org/10.1016/j.quascirev.2013.05.024

Filion, L., Payette, S., Gauthier, L., & Boutin, Y. (1986), Light rings in subarctic conifers as a dendrochronological tool. *Quaternary Research*, *26*(2), 272–279. https://doi.org/10.1016/0033-5894(86)90111-0

Fischer, E. M., Luterbacher, J., Zorita, E., Tett, S., Casty, C., & Wanner, H. (2007). European climate response to tropical volcanic eruptions over the last half millennium. *Geophysical Research Letters*, *34*(5). https://doi.org/10.1029/2006GL027992

Fonti, P., von Arx, G., García-González, I., Eilmann, B., Sass-Klaassen, U., Gärtner, H., et al. (2010). Studying global change through investigation of the plastic responses of xylem anatomy in tree rings. *New Phytologist*, *185*(1), 42–53.

Frank, D. C., Büntgen, U., Böhm, R., Maugeri, M., & Esper, J. (2007). Warmer early instrumental measurements versus colder reconstructed temperatures: shooting at a moving target. *Quaternary Science Reviews*, *26*(25–28), 3298–3310.

Fritts, H. (1976). *Tree rings and climate*. Academic Press.

Fritts, H. C., Vaganov, E. A., Sviderskaya, I. V., & Shashkin, A. V. (1991). Climatic variation and tree-ring structure in conifers: Empirical and mechanistic models of tree-ring width, number of cells, cell size, cell-wall thickness and wood density. *Climate Research*, *1*, 97–116.

Gärtner, H., & Schweingruber, F. (2013). Microscopic preparation techniques for plant stem analysis (pp. 83, Vol. 34). Remagen: Kessel Publishing House.

Gindl, W., Grabner, M., & Wimmer, R. (2000). The influence of temperature on latewood lignin content in treeline Norway spruce compared with maximum density and ring width. *Trees*, *14*(7), 409–414. https://doi.org/10.1007/s004680000057

Grattan, J., Durand, M., & Taylor, S. (2003). Illness and elevated human mortality in Europe coincident with the Laki fissure eruption. *Geological Society, London, Special Publications*, *213*(1), 401–414. https://doi.org/10.1144/GSL.SP.2003.213.01.24

Gregory, R. A. (1971). Cambial activity in Alaskan white spruce. *American Journal of Botany*, *58*(2), 160–171. https://doi.org/10.1002/j.1537-2197.1971.tb09959.x

Gu, L., Baldocchi, D. D., Wofsy, S. C., Munger, J. W., Michalsky, J. J., Urbanski, S. P., & Boden, T. A. (2003). Response of a deciduous forest to the Mount Pinatubo eruption: Enhanced photosynthesis. *Science*, *299*(5615), 2035–2038.

Guillet, S., Corona, C., Stoffel, M., Khodri, M., Lavigne, F., Ortega, P., et al. (2017). Climate response to the Samalas volcanic eruption in 1257 revealed by proxy records. *Nature Geoscience*, *10*(2), 123–128. https://doi.org/10.1038/ngeo2875

Hakim, G. J., Emile-Geay, J., Steig, E. J., Noone, D., Anderson, D. M., Tardif, R., et al. (2016), The last millennium climate reanalysis project: Framework and first results, *Journal of Geophysical Research: Atmospheres*, *121*(12), 6745–6764. https://doi.org/10.1002/2016JD024751

Harris, I., Jones, P. D., Osborn, T. J., & Lister, D. H. (2014). Updated high-resolution grids of monthly climatic observations–the CRU TS3. 10 dataset. *International Journal of Climatology*, *34*(3), 623–642.

Helama, S., L. Arppe, J. Uusitalo, J. Holopainen, H. M. Mäkelä, H. Mäkinen, et al. (2018). Volcanic dust veils from sixth century tree-ring isotopes linked to reduced irradiance, primary production and human health. *Scientific Reports*, *8*(1), 1–12.

Jacoby, G., Workman, K. W., & D'Arrigo, R. (1999). Laki eruption of 1783, tree rings, and disaster for northwest Alaska Inuit. *Quaternary Science Reviews*, *18*(12), 1365–1371. https://doi.org/10.1016/s0277-3791(98)00112-7

Kalnay, E., Kanamitsu, M., Kistler, R., Collins, W., Deaven, D., Gandin, L., et al. (1996). The NCEP/NCAR 40-year Reanalysis project. *Bulletin of the American Meteorological Society*, *77*(3), 437–471.

Körner, C. (1998). A re-assessment of high elevation treeline positions and their explanation. *Oecologia*, *115*(4), 445–459.

Körner, C. (2003). Carbon limitation in trees. *Journal of Ecology*, *91*(1), 4–17.

Körner, C. (2015). Paradigm shift in plant growth control. *Current Opinion in Plant Biology*, *25*, 107–114. https://doi.org/10.1016/j.pbi.2015.05.003

Krakauer, N. Y., & Randerson, J. T. (2003). Do volcanic eruptions enhance or diminish net primary production? Evidence from tree rings. *Global Biogeochemical Cycles*, *17*(4).

Kravitz, B., & Robock, A. (2011). Climate effects of high-latitude volcanic eruptions: Role of the time of year. *Journal of Geophysical Research: Atmospheres*, *116*(D1). https://doi.org/10.1029/2010JD014448

Lange, J., Carrer, M., Pisaric, M. F., Porter, T. J., Seo, J.-W., Trouillier, M., et al. (2020). Moisture-driven shift in the climate sensitivity of white spruce xylem anatomical traits is coupled to large-scale oscillation patterns across northern treeline in northwest North America. *Global Change Biology*, *26*(3), 1842–1856. https://doi.org/10.1111/gcb.14947

Lawrimore, J. H., Menne, M. J., Gleason, B. E., Williams, C. N., Wuertz, D. B., Vose, R. S., et al. (2011). An overview of the Global Historical Climatology Network monthly mean temperature data set, version 3. *Journal of Geophysical Research*, *116*(D19). https://doi.org/10.1029/2011JD016187

LeGrande, A. N., & Anchukaitis, K. J. (2015). Volcanic eruptions and climate. *Past Global Change Magazine*, *23*(2), 46–47. http://dx.doi.org/10.22498/pages.23.2.46

LeGrande, A. N., Tsigaridis, K., & Bauer, S. E. (2016). Role of atmospheric chemistry in the climate impacts of stratospheric volcanic injections. *Nature Geoscience*, *9*(9), 652–655.

Liu, Z., Yoshimura, K., Buenning, N. H., Jian, Z., & Zhao, L. (2017). The response of winter Pacific North American pattern to strong volcanic eruptions. *Climate Dynamics*, *48*(11–12), 3599–3614.

Luterbacher, J., Dietrich, D., Xoplaki, E., Grosjean, M., & Wanner, H. (2004). European seasonal and annual temperature variability, trends, and extremes since 1500. *Science*, *303*(5663), 1499–1503.

Mann, G. W., Dhomse, S., Deshler, T., Timmreck, C., Schmidt, A., Neely, R., et al. (2015). Evolving particle size is the key to improved volcanic forcings. *Past Global Changes Magazine*, *23*, 52–53.

Marshall, L., Johnson, J. S., Mann, G. W., Lee, L., Dhomse, S. S., Regayre, L., et al. (2019). Exploring how eruption source parameters affect volcanic radiative forcing using statistical emulation. *Journal of Geophysical Research: Atmospheres*, *124*(2), 964–985. https://doi.org/10.1029/2018JD028675

Marsh, D. R., Mills, M. J., Kinnison, D. E., Lamarque, J.-F., Calvo, N., & Polvani, L. M. (2013). Climate change from 1850 to 2005 simulated in CESM1 (WACCM). *Journal of Climate*, *26*(19), 7372–7391.

Masson-Delmotte, V., Schulz, M., Abe-Ouchi, A., Beer, J., Ganopolski, A., Rouco, J. G., et al. (2013). Information from Paleoclimate Archives. In *Climate change 2013: The physical science basis. Contribution of working group I to the fifth assessment report of the intergovernmental panel on climate change*, T. F. Stocker, D. Qin, G.-K. Plattner, M. Tignor, S. Allen, J. Boschung, et al. (Eds) (pp. 383–464). Cambridge, United Kingdom and New York, NY, USA: Cambridge University Press.

Matisons, R., Gärtner, H., Elferts, D., Kārkliņa, A., Adamovičs, A., & Jansons, A. (2020). Occurrence of 'blue' and 'frost' rings reveal frost sensitivity of eastern Baltic provenances of Scots pine. *Forest Ecology and Management*, *457*(117), 729.

McConnell, J. R., Sigl, M., Plunkett, G., Burke, A., Kim, W. M., Raible, C. C., et al. (2020). Extreme climate after massive eruption of Alaska's Okmok volcano in 43 BCE and effects on the late Roman Republic and Ptolemaic Kingdom. *Proceedings of the National Academy of Sciences*, *117*(27), 15443–15449. https://doi.org/10.1073/pnas.2002722117

Mills, M. J., Richter, J. H., Tilmes, S., Kravitz, B., MacMartin, D. G., Glanville, A. A., et al. (2017). Radiative and chemical response to interactive stratospheric sulfate aerosols in fully coupled CESM1(WACCM). *Journal of Geophysical Research: Atmospheres*, *122*(23), 13061–13078, https://doi.org/10.1002/2017jd027006

Mills, M. J., Schmidt, A., Easter, R., Solomon, S., Kinnison, D. E., Ghan, S. J., et al. (2016). Global volcanic aerosol properties derived from emissions, 1990–2014, using CESM1 (WACCM). *Journal of Geophysical Research: Atmospheres*, *121*(5), 2332–2348. https://doi.org/10.1002/2015JD024290

Mork, E. (1928). Die qualität dês fichtenholzes unter besonderer rucksichtnahme auf schleif-und papierholz. *Papier-fabrikant*, *26*, 741–747.

Nemani, R. R. (2003). Climate-driven increases in global terrestrial net primary production from 1982 to 1999. *Science*, *300*(5625), 1560–1563. https://doi.org/10.1126/science.1082750

Newfield, T. P. (2018). The climate downturn of 536–50. In *The palgrave handbook of climate history* (pp. 447–493). Springer.

Newhall, C., Self, S., & Robock, A. (2018). Anticipating future volcanic explosivity index (VEI) 7 eruptions and their chilling impacts. *Geosphere*, *14*(2), 572–603.

Oman, L., Robock, A., Stenchikov, G. L., Thordarson, T., Koch, D., Shindell, D. T., & Gao, C. (2006). Modeling the distribution of the volcanic aerosol cloud from the 1783–1784 Laki eruption. *Journal of Geophysical Research: Atmospheres*, *111*(D12). https://doi.org/10.1029/2005JD006899

Oquilluk, W. A. (1973). *People of Kauwerak: Legends of the northern Eskimo*. Alaska Pacific University Press.

Pausata, F. S. R., Grini, A., Caballero, R., Hannachi, A., & Seland, Ø. (2015). High-latitude volcanic eruptions in the Norwegian Earth System Model: the effect of different initial conditions and of the ensemble size. *Tellus B: Chemical and Physical Meteorology*, *67*(1), 26728. https://doi.org/10.3402/tellusb.v67.26728

Peters, R. L., Balanzategui, D., Hurley, A. G., von Arx, G., Prendin, A. L., Cuny, H. E., et al. (2018). RAPTOR: Row and position tracheid organizer in R. *Dendrochronologia*, *47*, 10–16. https://doi.org/10.1016/j.dendro.2017.10.003

Peterson, T. C., & Vose, R. S. (1997). An overview of the Global Historical Climatology Network temperature database. *Bulletin of the American Meteorological Society*, *78*(12), 2837–2850.

Piermattei, A., Crivellaro, A., Carrer, M., & Urbinati, C. (2015). The "blue ring": Anatomy and formation hypothesis of a new tree-ring anomaly in conifers. *Trees*, *29*(2), 613–620.

Pinto, J. P., Turco, R. P., & Toon, O. B. (1989). Self-limiting physical and chemical effects in volcanic eruption clouds. *Journal of Geophysical Research*, *94*(D8), 11165–11174. https://doi.org/10.1029/JD094iD08p11165

Prendin, A. L., Petit, G., Carrer, M., Fonti, P., Björklund, J., & von Arx, G. (2017). New research perspectives from a novel approach to quantify tracheid wall thickness. *Tree Physiology*, *37*(7), 976–983. https://doi.org/10.1093/treephys/tpx037

R Core Team (2019). *R: A language and environment for statistical computing*. Vienna, Austria: R Foundation for Statistical Computing.

Rathgeber, C. B. K., Cuny, H. E., & Fonti, P. (2016). Biological basis of tree-ring formation: A crash course. *Frontiers in Plant Science*, *7*. https://doi.org/10.3389/fpls.2016.00734

Robock, A. (2000), Volcanic eruptions and climate, *Reviews of Geophysics*, *38*(2), 191–219, https://doi.org/10.1029/1998rg000054

Robock, A. (2005). Cooling following large volcanic eruptions corrected for the effect of diffuse radiation on tree rings. *Geophysical Research Letters*, *32*(6). https://doi.org/10.1029/2004gl022116

Robock, A., MacMartin, D. G., Duren, R., & Christensen, M. W. (2013). Studying geoengineering with natural and anthropogenic analogs. *Climatic Change*, *121*(3), 445–458.

Roderick, M. L., Farquhar, G. D., Berry, S. L., & Noble, I. R. (2001). On the direct effect of clouds and atmospheric particles on the productivity and structure of vegetation. *Oecologia*, *129*(1), 21–30.

Rossi, S., Anfodillo, T., Čufar, K., Cuny, H. E., Deslauriers, A., Fonti, P., et al. (2016). Pattern of xylem phenology in conifers of cold ecosystems at the Northern Hemisphere. *Global Change Biology*, *22*(11), 3804–3813. https://doi.org/10.1111/gcb.13317

Rossi, S., Deslauriers, A., & Anfodillo, T. (2006). Assessment of cambial activity and xylogenesis by microsampling tree species: An example at the alpine timberline. *IAWA Journal*, *27*(4), 383–394.

Rossi, S., Deslauriers, A., Griçar, J., Seo, J.-W., Rathgeber, C. B., Anfodillo, T., et al. (2008). Critical temperatures for xylogenesis in conifers of cold climates. *Global Ecology and Biogeography*, *17*(6), 696–707. https://doi.org/10.1111/j.1466-8238.2008.00417.x

Rossi, S., Girard, M.-J., & Morin, H. (2014). Lengthening of the duration of xylogenesis engenders disproportionate increases in xylem production. *Global Change Biology*, *20*(7), 2261–2271. https://doi.org/10.1111/gcb.12470

Rossi, S., Morin, H., & Deslauriers, A. (2012). Causes and correlations in cambium phenology: Towards an integrated framework of xylogenesis. *Journal of Experimental Botany*, *63*(5), 2117–2126.

Schmidt, A., Carslaw, K., Mann, G. W., Wilson, M., Breider, T., Pickering, S., et al. (2010). The impact of the 1783–1784 AD Laki eruption on global aerosol formation processes and cloud condensation nuclei. *Atmospheric Chemistry and Physics*, *10*(13), 6025–6041.

Schmidt, G. A., Jungclaus, J. H., Ammann, C. M., Bard, E., Braconnot, P., Crowley, T. J., et al. (2012). Climate forcing reconstructions for use in PMIP simulations of the Last Millennium (v1.1). *Geoscientific Model Development*, *5*(1), 185–191.

Schmidt, A., M. J. Mills, S. Ghan, J. M. Gregory, R. P. Allan, T. Andrews, et al. (2018). Volcanic radiative forcing from 1979 to 2015. *Journal of Geophysical Research: Atmospheres*, *123*(22), 12491–12508. https://doi.org/10.1029/2018JD028776

Schmidt, A., Ostro, B., Carslaw, K. S., Wilson, M., Thordarson, T., Mann, G. W., et al. (2011). Excess mortality in Europe following a future Laki-style Icelandic eruption. *Proceedings of the National Academy of Sciences*, *108*(38), 15710–15715. https://doi.org/10.1073/pnas.1108569108

Schneider, D. P., Ammann, C. M., Otto-Bliesner, B. L., & Kaufman, D. S. (2009). Climate response to large, high-latitude and low-latitude volcanic eruptions in the Community Climate System Model. *Journal of Geophysical Research*, *114*(D15). https://doi.org/10.1029/2008jd011222

Schneider, L., Smerdon, J. E., Pretis, F., Hartl-Meier, C., & Esper, J. (2017). A new archive of large volcanic events over the past millennium derived from reconstructed summer temperatures. *Environmental Research Letters*, *12*(9), 094005. https://doi.org/10.1088/1748-9326/aa7a1b

Schove, D. J. (1954). Summer temperatures and tree-rings in North-Scandinavia AD 1461–1950. *Geografiska Annaler*, *36*(1–2), 40–80.

Sigl, M., Winstrup, M., McConnell, J. R., Welten, K. C., Plunkett, G., Ludlow, F., et al. (2015). Timing and climate forcing of volcanic eruptions for the past 2,500 years. *Nature*, *523*(7562), 543–549. https://doi.org/10.1038/nature14565

Stenchikov, G., Hamilton, K., Stouffer, R. J., Robock, A., Ramaswamy, V., Santer, B., et al. (2006). Arctic Oscillation response to volcanic eruptions in the IPCC AR4 climate models. *Journal of Geophysical Research*, *111*(D7). https://doi.org/10.1029/2005JD006286

Stevenson, S., Fasullo, J. T., Otto-Bliesner, B. L., Tomas, R. A., & Gao, C. (2017). Role of eruption season in reconciling model and proxy responses to tropical volcanism. *Proceedings of the National Academy of Sciences*, *114*(8), 1822–1826. https://doi.org/10.1073/pnas.1612505114

Stevenson, D. S., Johnson, C. E., Highwood, E. J., Gauci, V., Collins, W. J., & Derwent, R. G. (2003). Atmospheric impact of the 1783–1784 Laki eruption: Part I chemistry modelling. *Atmospheric Chemistry and Physics*, *3*(3), 487–507. https://doi.org/10.5194/acp-3-487-2003

Stoffel, M., Khodri, M., Corona, C., Guillet, S., Poulain, V., Bekki, S., et al. (2015). Estimates of volcanic-induced cooling in the Northern Hemisphere over the past 1,500 years. *Nature Geoscience*, *8*(10), 784–788. https://doi.org/10.1038/ngeo2526

Szeicz, J. M. (1996). White spruce light rings in northwestern Canada. *Arctic and Alpine Research*, *28*(2), 184–189. https://doi.org/10.1080/00040851.1996.12003164

Tardif, R., Hakim, G. J., Perkins, W. A., Horlick, K. A., Erb, M. P., Emile-Geay, J., et al. (2019). Last Millennium Reanalysis with an expanded proxy database and seasonal proxy modeling. *Climate of the Past*, *15*(4), 1251–1273. https://doi.org/10.5194/cp-15-1251-2019

Thordarson, T., & Self, S. (2003). Atmospheric and environmental effects of the 1783–1784 Laki eruption: A review and reassessment. *Journal of Geophysical Research*, *108*(D1). https://doi.org/10.1029/2001jd002042

Timmreck, C. (2012). Modeling the climatic effects of large explosive volcanic eruptions. *Wiley Interdisciplinary Reviews: Climate Change*, *3*(6), 545–564. https://doi.org/10.1002/wcc.192

Timmreck, C., Graf, H.-F., Lorenz, S. J., Niemeier, U., Zanchettin, D., Matei, D., et al. (2010). Aerosol size confines climate response to volcanic super-eruptions, *Geophysical Research Letters*, *37*(24). https://doi.org/10.1029/2010GL045464

Timmreck, C., Lorenz, S. J., Crowley, T. J., Kinne, S., Raddatz, T. J., Thomas, M. A., et al. (2009). Limited temperature response to the very large AD 1258 volcanic eruption. *Geophysical Research Letters*, *36*(21). https://doi.org/10.1029/2009GL040083

Tingley, M. P., & Huybers, P. (2013). Recent temperature extremes at high northern latitudes unprecedented in the past 600 years. *Nature*, *496*(7444), 201–205. https://doi.org/10.1038/nature11969

Tingley, M. P., Stine, A. R., & Huybers, P. (2014). Temperature reconstructions from tree-ring densities overestimate volcanic cooling. *Geophysical Research Letters*, *41*(22), 7838–7845. https://doi.org/10.1002/2014gl061268

Tolwinski-Ward, S., Anchukaitis, K. J., & Evans, M. N. (2013). Bayesian parameter estimation and interpretation for an intermediate model of tree-ring width. *Climate of the Past*, *9*(4), 1481–1493.

Toohey, M., Krüger, K., Schmidt, H., Timmreck, C., Sigl, M., Stoffel, M., & Wilson, R. (2019). Disproportionately strong climate forcing from extratropical explosive volcanic eruptions. *Nature Geoscience*, *12*(2), 100–107.

Toohey, M., & Sigl, M. (2017). Volcanic stratospheric sulfur injections and aerosol optical depth from 500 BCE to 1900 CE. *Earth System Science Data*, *9*(2), 809–831. https://doi.org/10.5194/essd-9-809-2017

Vaganov, E. A., Anchukaitis, K. J., & Evans, M. N. (2011). How well understood are the processes that create dendroclimatic records? A mechanistic model of the climatic control on conifer tree-ring growth gynamics. In Hughes, M. K., Swetnam, T. W., & Diaz, H. F., Dendroclimatology: Progress and prospects, developments in paleoenvironmental research (pp. 37–75, Vol 11). Springer Netherlands, https://doi.org/10.1007/978-1-4020-5725-0_3

Vaganov, E. A., Hughes, M. K., Kirdyanov, A. V., Schweingruber, F. H., & Silkin, P. P. (1999). Influence of snowfall and melt timing on tree growth in subarctic Eurasia. *Nature*, *400*, 149–151.

Vaganov, E. A., Hughes, M. K., & Shashkin, A. V. (2006). Growth Dynamics of Conifer Tree Rings: Images of past and future environments (Vol. 183). Springer Science & Business Media.

Vaganov, E. A., Sviderskaya, I. V., & Kondratyeva, E. N. (1990). Climatic conditions and tree ring structure: simulation model of trachidogram (in Russian). *Lesovedenie*, *2*, 37–45.

Vermunt, B., Cuddington, K., Sobek-Swant, S., Crosthwaite, J. C., Lyons, D. B., & Sinclair, B. J. (2012). Temperatures experienced by wood-boring beetles in the under-bark microclimate. *Forest Ecology and Management*, *269*, 149–157. https://doi.org/10.1016/j.foreco.2011.12.019

von Arx, G., & Carrer, M. (2014). ROXAS–A new tool to build centuries-long tracheid-lumen chronologies in conifers. *Dendrochronologia*, *32*(3), 290–293. https://doi.org/10.1016/j.dendro.2013.12.001

von Arx, G., Crivellaro, A., Prendin, A. L., Čufar, K., & Carrer, M. (2016). Quantitative wood anatomy—practical guidelines. *Frontiers in Plant Science*, *7*. https://doi.org/10.3389/fpls.2016.00781

Wilson, R., Anchukaitis, K., Briffa, K. R., Büntgen, U., Cook, E. R., D'Arrigo, R., et al. (2016). Last millennium northern hemisphere summer temperatures from tree rings: Part i: The long term context. *Quaternary Science Reviews*, *134*, 1–18. https://doi.org/10.1016/j.quascirev.2015.12.005

Witham, C., & Oppenheimer, C. (2004). Mortality in England during the 1783-4 Laki craters eruption. *Bulletin of Volcanology*, *67*, 15–26. https://doi.org/10.1007/s00445-004-0357-7

Yasue, K., Funada, R., Kobayashi, O., & Ohtani, J. (2000). The effects of tracheid dimensions on variations in maximum density of Picea glehnii and relationships to climatic factors. *Trees - Structure and Function*, *14*, 223–229. https://doi.org/10.1007/PL00009766

Zambri, B., Robock, A., Mills, M. J., & Schmidt, A. (2019a). Modeling the 1783–1784 Laki eruption in Iceland: 2. Climate impacts. *Journal of Geophysical Research: Atmospheres*, *124*(13), 6770–6790. https://doi.org/10.1029/2018jd029554

Zambri, B., Robock, A., Mills, M. J., & Schmidt, A. (2019b). Modeling the 1783–1784 Laki eruption in Iceland: 1. Aerosol evolution and global stratospheric circulation impacts. *Journal of Geophysical Research: Atmospheres*, *124*(13), 6750–6769. https://doi.org/10.1029/2018jd029553

Zanchettin, D., Timmreck, C., Graf, H.-F., Rubino, A., Lorenz, S., Lohmann, K., et al. (2012). Bi-decadal variability excited in the coupled ocean–atmosphere system by strong tropical volcanic eruptions. *Climate Dynamics*, *39*(1), 419–444.

Zhu, F., Emile-Geay, J., Hakim, G. J., King, J., & Anchukaitis, K. J. (2020). Resolving the differences in the simulated and reconstructed temperature response to volcanism. *Geophysical Research Letters*, *47*(8). https://doi.org/10.1029/2019gl086908

Ziaco, E., Biondi, F., Rossi, S., & Deslauriers, A. (2014). Climatic influences on wood anatomy and tree-ring features of Great Basin conifers at a new mountain observatory. *Applications in Plant Sciences*, *2*(10), 1400054. https://doi.org/10.3732/apps.1400054